# VLA-4 suppression by senescence signals regulates meningeal immunity and leptomeningeal metastasis

Jiaqian Li[1,2,7], Di Huang[1,2,7], Bingxi Lei[5,7], Jingying Huang[1,2], Qiyi Zhao[3,6], Shicheng Su[1,2,3,4*], Ying Wang[1,2*]

**Affiliations**

[1]Guangdong Provincial Key Laboratory of Malignant Tumor Epigenetics and Gene Regulation, Medical Research Center, Sun Yat-Sen Memorial Hospital, Sun Yat-Sen University, Guangzhou 510120, China.

[2]Breast Tumor Center, Sun Yat-Sen Memorial Hospital, Sun Yat-Sen University, Guangzhou 510120, China.

[3]Department of Infectious Diseases, Third Affiliated Hospital, Sun Yat-Sen University, Guangzhou 510630, China.

[4]Department of Immunology, Zhongshan School of Medicine, Sun Yat-Sen University, Guangzhou 510080, China.

[5]Department of Neurosurgery, Sun Yat-Sen Memorial Hospital, Sun Yat-Sen University, Guangzhou 510120, China.

[6]Guangdong Provincial Key Laboratory of Liver Disease Research, the Third Affiliated Hospital, Sun Yat-Sen University, Guangzhou 510630, China.

[7]These authors contributed equally to this work.

***For Correspondence**: sushch@mail.sysu.edu.cn; wangy556@mail.sysu.edu.cn.

**Competing interest**: The authors declare that no competing interests exist.

## Abstract

Leptomeningeal metastasis is associated with dismal prognosis and has few treatment options. However, very little is known about the immune response to leptomeningeal metastasis. Here, by establishing an immunocompetent mouse model of breast cancer leptomeningeal metastasis, we found that tumor-specific $CD8^+$ T cells were generated in deep cervical lymph nodes (dCLNs) and played an important role in controlling leptomeningeal metastasis. Mechanistically, T cells in dCLNs displayed a senescence phenotype and their recruitment was impaired in mice bearing cancer cells that preferentially colonized in leptomeningeal space. Upregulation of p53 suppressed the transcription of VLA-4 in senescent dCLN T cells and consequently inhibited their migration to the leptomeningeal compartment. Clinically, $CD8^+$ T cells from cerebrospinal fluid of patients with leptomeningeal metastasis exhibited senescence and VLA-4 downregulation. Collectively, our findings demonstrated that $CD8^+$ T cell immunosenescence drives leptomeningeal metastasis.

## Keywords

Leptomeningeal metastasis, meningeal immunity, deep cervical lymph nodes, immunosenescence, VLA-4

## Introduction

Brain metastasis is associated with one of the worst clinical outcomes and has few therapeutic options(1). The brain contains two distinctive compartments— parenchyma mainly consisting of cells and leptomeninges filled with cerebrospinal fluid (CSF) (2). Many brain parenchymal cells can be found nowhere else in the body, including neurons, astrocytes and microglia. Despite tremendous progress has been made in understanding the interaction between tumor cells and resident cells in parenchymal metastasis, very little is known about the unique microenvironment of leptomeningeal metastasis (LM)(3). LM, which is caused by cancer cells invading the leptomeninges, or cerebral-spinal fluid-filled spaces, represents the worst outcome of cancer patients(4,5). Despite the development of diagnostic techniques and advances in cancer treatment, the incidence of breast cancer with leptomeningeal metastasis increases, ranging between 3% to 16%(6). LM is a fatal complication with dismal prognosis. Its median survival from detection is as low as 18 weeks, and 1- year survival is about 15%(7).

Access of circulating immune cells to the brain is limited by the blood–brain barrier (BBB). Therefore, the brain has previously been considered as an immune-privileged organ. Recently, the paradigm has shifted as functional lymphatic vessels have been identified in meninges. Immune cells and antigens in central nervous system (CNS) can be drained to deep cervical lymph nodes (dCLNs) via meningeal lymphatic system(8). Ablation of lymphatic vessels reduces the interaction between brain-specific T cells and dendritic cells (DC), and alleviates disease progression in experimental allergic encephalomyelitis (EAE) mice(9), indicating that lymphatic drainage contributes to T cell activation in CNS. The very late activated Ag-4 (VLA-4) is a member of integrin family, which is widely known to mediate T cell adhesion to endothelium. In fact, VLA-4 acts as a key adhesion molecule in T-cell passage through the blood–brain barrier in EAE(10,11). However, their roles in CNS diseases are still poorly understood.

Cancer is often associated with ageing, as the incidences of most cancers rise dramatically in senior(12,13). Oncogene activation mediates tumor cells to adopt a senescence-associated secretory phenotype (SASP), which fosters chronic inflammatory milieus(14,15). Consequently, the ageing microenvironment induces senescence of T cells, which leads to immunosuppression in multiple types of maligancies(16). Furthermore, the tumor microenvironment (TME) can induce senescence of adoptively transferred tumor-specific T cells, and therefore develop a resistance to immunotherapy(17). However，whether immunosenescence contributes to the immunosuppression of meningeal immune response to tumors remains unreported. Here, we investigated how anti-tumor meningeal immunity is initiated and suppressed during leptomeningeal metastasis.

## Results

### Establishing a model of cancer leptomeningeal metastasis

To investigate the role of immunity in leptomeningeal metastasis, we used immunocompetent mice and employed a two-stage *in vivo* selection method to enrich breast cancer cells with leptomeningeal tropism. First, selecting the cancer cells that survived in the CSF. Second, selecting cancer cells from the resulting populations for hematogenous tropism to colonize the leptomeninges through intracarotid artery injection (Figure 1A). Briefly, mouse breast cancer cells (EO771 and 4T1) and lung cancer cells (LLC) stably expressing luciferase were inoculated into the cisterna magna of syngeneic mice C57BL/6 (EO771-luc, LLC-luc) or BALB/c (4T1-luc) (Figure 1A). Once leptomeningeal metastatic lesions were established, cancer cells were isolated from the meninges and cultured *ex vivo* to obtain intermediate sublines. Intermediate cells were then inoculated into intracarotid artery for hematogenous dissemination to meningeal space. Cancer cells in metastatic lesions of leptomeningeal space after 3 times of enrichment were selected as a highly leptomeningeal metastatic subline "LM-phenotype cells" (Figure 1A). To evaluate the leptomeningeal metastatic capacity of

this selected derivative, we performed bioluminescent imaging and animal MRI analysis after injection of EO771 LM-phenotype cells and their parental cells via intracarotid artery. Intense bioluminescence imaging (BLI) signals (Figure 1B-C) and hyperintense T1-weighted signals (Figure 1D) throughout tumors in the meningeal space demonstrated abundant neuro-anatomic metastases of mice injected with LM-phenotype cells, rather than the parental cells. Moreover, we confirmed the leptomeningeal localization of metastases by the immunohistochemical (Figure 1E—figure supplement 1A) and immunofluorescent staining (Figure 1F—figure supplement 1B). Furthermore, LM cell injection into the intracarotid artery significantly shortened animal survival compared to the parental cell (Figure 1G). Similar results were observed in mice injected with 4T1 LM phenotype cells (Figure supplement 1C-F) and LLC LM phenotype cells (Figure supplement 1G-J). Furthermore, principal component analysis (PCA) of the transcriptome confirmed that the gene expression profiles of EO771 parental, inter and LM-phenotype cells segregate independently (Figure 1H). Thus, there was a heterogeneity between LM population and its matched parental population.

**$CD8^+$ T cells constrain leptomeningeal metastasis**

Emerging data show that meningeal immunity plays a crucial role in various diseases (18), but how this CNS barrier operates immunologically under leptomeningeal metastasis remains poorly understood. We found that $CD45^+$ immune cells increased in mice injected with parental or LM cells, when compared with those injected with PBS, indicating that the meninges were inflamed after tumor inoculation. However, meningeal immune cell numbers in the presence of leptomeningeal metastasis dropped significantly in comparison with those injected with parental cells (Figure 2A). To further investigate the changes of meningeal immune repertoire during leptomeningeal metastasis, we analyzed the absolute numbers of meninge-infiltrating immune cells, including T cells, monocytes, microglia, myeloid cells and neutrophils(19). Interestingly, we observed that only T cells were markedly decreased in leptomeningeal

metastasis (Figure 2B—figure supplement 2A). To confirm the role of T lymphocytes in leptomeningeal metastasis, we injected EO771 LM-phenotype cells into *Rag2*$^{-/-}$ mice, which carry a targeted knockout mutation in recombination activating gene 2 (*Rag2*) and therefore lack mature T or B cells (20). Compared with wild type (WT) C57BL/6 mice, accelerated intracranial tumor progression was observed in the *Rag2*$^{-/-}$ mice when LM-phenotype cells were injected via intracarotid arteries, which was evaluated by bioluminescent signals (Figure 2C-D). Similarly, we injected 4T1 LM-phenotype cells into the immunodeficient nude mice and immunocompetent BALB/c mice, and observed that tumor formation was significantly enhanced in nude mice (Figure supplement 2B-C). To assess which subset of T cells contributes to constrain leptomeningeal metastasis, we depleted $CD4^+$ and $CD8^+$ T cells in immunocompetent C57BL/6 mice via anti-CD4 (α-CD4) and anti-CD8 neutralizing antibodies (α-CD8) respectively. Analysis of the leptomeningeal metastases by histopathology, we found that the mice without $CD8^+$ T cells dramatically increased intracranial tumor growth compared with IgG neutralization (Figure 2E—figure supplement 2D). By contrast, depletion of $CD4^+$ T cells even exhibited slight tumor regression, although the difference didn't reach statistical significance (Figure 2E—figure supplement 2D). These results suggested that $CD8^+$ T cells play an important role in constraining intracranial tumor growth.

Most of the immune surveillance takes place in the tumor draining lymph nodes (TDLN) due to its cellular composition and proximity to the primary tumor(21). It has been reported that deep cervical lymph nodes (dCLNs) communicate with meningeal lymphatics directly(8). Evans blue, which is widely used as a marker of the blood-brain barrier integrity, can be preferentially drained via the lymphatics(22). Therefore, to visualize CNS lymphatic drainage, we injected Evans blue into the cisterna magna and detected the presence of dye in dCLNs 30 minutes later (Figure 2F). Furthermore, we isolated $CD4^+$ and $CD8^+$ T cells from dCLNs of WT mice two weeks after EO771 cell injection. These isolated T cells were adoptively transferred into syngeneic *Rag2*$^{-/-}$ mice,

164 respectively, followed by LM-phenotype cell inoculation (Figure 2G). Interestingly,
165 intracranial tumors arising in *Rag2*$^{-/-}$ mice was much smaller when receiving transferred
166 CD8$^{+}$ T cells, but not CD4$^{+}$ T cells (Figure 2H—figure supplement 2E). More
167 importantly, mice receiving CD8$^{+}$ T cells had longer overall survival than those
168 receiving CD4$^{+}$ T cells or PBS (Figure 2I). These data suggested that CD8$^{+}$ T cells are
169 crucial effectors in controlling leptomeningeal metastasis.
170
171 **dCLNs generate tumor-specific CD8$^{+}$ T cells against leptomeningeal metastasis**
172 Activation of tumor-specific CD8$^{+}$ T cells depends on tumor antigen presentation by
173 DCs, which is the fundamental step that launches T cell response against tumor(23,24).
174 To explore whether tumor-specific CD8$^{+}$ T cells were primed by DCs in dCLN, we
175 firstly examined the antigen processing of DCs. We inoculated EO771 breast tumor
176 cells with ectopic expression of chicken ovalbumin (OVA) (EO771-OVA) into the
177 cisterna magna of C57BL/6 mice and isolated the CD11c$^{+}$ DCs from the draining
178 dCLNs, non-draining inguinal LNs and spleen 7 days later. Interestingly, OVA
179 peptide/MHC class I complex, SIINFEKL/H2-Kb, was only detected on CD11c$^{+}$ DCs
180 in dCLNs but not the ones in inguinal LNs and spleen (Figure 3A—figure supplement
181 3A, B). Furthermore, we employed H-2-Kb-OVA/SIINFEKL pentamer staining to
182 detect the generation of OVA-specific CD8$^{+}$ T cells. Interestingly, we observed that a
183 significant proportion of OVA/SIINFEKL pentamer$^{+}$ CD8$^{+}$ T cells was detected in the
184 dCLNs of mice injected with EO771-OVA cells, but not in the mice injected with PBS,
185 wild type EO771 (EO771 WT) and EO771 with an irrelevant antigen glycoprotein B
186 (EO771-gB) cells (Figure 3B—figure supplement 3C). Moreover, CD11c$^{+}$ DCs were
187 subsequently isolated from dCLNs, and then co-cultured with naïve CD8$^{+}$ T cells
188 isolated from the spleens of OT-1 mice *in vitro* (Figure 3C). Analysis of OT-1 T cell
189 priming revealed that only DCs from mice receiving EO771-OVA inoculation could
190 expand OT-1 T cells (Figure 3D—figure supplement 3D) and induce a significant
191 increase in IFN-γ production (Figure 3E—figure supplement 3E) of OT-1 T cells.
192

Meningeal lymphatics act as an avenue for CNS drainage and immune cell trafficking(25). We performed the surgical ligation of the lymphatic afferent to the dCLNs, which could disrupt the meningeal lymphatic drainage. A week after the surgery, sham or ligation group were inoculated with EO771-OVA cells, respectively (Figure 3F). Determined by the expression of SIINFEKL/H2-Kb complex on the surface of $CD11c^+$ dCLN DCs, antigen processing was impaired in the mice receiving surgical ligation (Figure 3G—figure supplement 3F). In addition, the proliferation (Figure 3H — figure supplement 3G) and IFN-γ production (Figure 3I — figure supplement 3H) of OT-1 T cells primed by dCLN DCs were diminished. Collectively, dCLNs could generate tumor-specific $CD8^+$ T cells.

**dCLN $CD8^+$ T cells exhibit senescence in leptomeningeal metastasis**

Adaptive immune response against tumor was provoked by antigen-specific $CD8^+$ T cells(26). Whether $CD8^+$ T cells controlling metastasis in metastatic locations or affecting dissemination of cancer cells is not clear. We first evaluated whether $CD8^+$ T cells control tumor metastasis in affecting dissemination of cancer cells by analyzing disseminated tumor cells (DTCs) in peripheral blood of C57BL/6 mice injected with EO771-luc parental or LM cells. The DTCs in the blood were defined as $CD45^-$ $luciferase^+$ cells by flow cytometry (Figure supplement 4A). We found that the percentages of DTCs were not significantly different between these two groups (Figure supplement 4B-C). Moreover, we injected EO771-luc LM cells into *Rag2*$^{-/-}$ mice and transferred $CD8^+$ T cells later. We found that $CD8^+$ T cell transfusion did not influence the percentages of DTCs in the peripheral blood (Figure supplement 4D). These data suggested that $CD8^+$ T cells did not affect the dissemination of cancer cells, probably the metastatic lesion. Then we observed that in the meninge, the number of $CD8^+$ T cells of mice injected with EO771 LM-phenotype cells (LM-$CD8^+$ T cells) was much lower than the one in mice injected with parental cells (Parental-$CD8^+$ T cells) (Figure 4A, B—figure supplement 4E). Then, we further investigated the reason for the drop of $CD8^+$ T cell count in the meninges. It's well known that tumor-specific $CD8^+$ T cells

were primed by DCs in dCLNs, migrated to meninges, and recognized and lysed tumor cells (27). Therefore, we evaluated the number of $CD8^+$ T cells in dCLNs of mice injected with LM cells and parental cells. Interestingly, we found that the absolute count of LM-$CD8^+$ T cells in dCLNs was significantly lower than Parental-$CD8^+$ T cells (Figure 4C, D—figure supplement 4F). Moreover, the proliferation of LM-$CD8^+$ T cells in dCLNs was significantly decreased, compared with the dCLN Parental-$CD8^+$ T cells, determined by flow cytometric analysis of CD8 and Ki-67 co-staining (Figure 4E—figure supplement 4G). These data suggested that the decreased proliferation of $CD8^+$ T cells in dCLNs was one of the reasons of low infiltration of $CD8^+$ T cells in leptomeningeal metastatic lesion.

Since T cell proliferation is often impaired during apoptosis and senescence, we evaluated the apoptosis and senescence of LM- and Parental-$CD8^+$ T cells in dCLNs. Determined by the apoptotic marker, cleaved caspase 3 expression, by flow cytometric analysis, LM- and Parental-$CD8^+$ T cells have equivalent amount of cleaved caspase 3 (Figure 4F—figure supplement 4H), indicating that apoptosis is not the major cause contributing to the impaired proliferation of T cells. On the other hand, senescence represents a stress response in which cells withdraw from the cell cycle and lose the capability to proliferate in response to growth factors or mitogens(28). We detected the distinct increased expression of senescence markers p53 and p21 in dCLN LM- $CD8^+$ T cells, compared with dCLN Parental- $CD8^+$ T cells (Figure 4G, source data 1). Moreover, the percentage of senescence-associated β-galactosidase (SA-β-gal) positive T cells was higher in the LM-$CD8^+$ T cells (Figure 4H, I). Similar results were also found in $CD8^+$ T cells in dCLNs of the mice injected with LLC LM-phenotype cells (Figure supplement 4I-K). Collectively, $CD8^+$ T cells in dCLNs of mice bearing LM exhibit senescence.

**Downregulation of VLA-4 in senescent $CD8^+$ T cells impairs their trafficking to meninges**

Besides the proliferation, we also evaluated the trafficking ability of dCLN LM- and Parental- $CD8^+$ T cells. We isolated the dCLN $CD8^+$ T cells, labeled with CFSE and injected into the tail vein of recipient mice. Two-photon live imaging showed that the migration of LM- $CD8^+$ T cells to meninges *in vivo* was significantly less than Parental-$CD8^+$ T cells (Figure 5A—figure supplement 5A), suggesting that $CD8^+$ T cells displayed impaired trafficking ability to meninges under leptomeningeal metastasis.

The very late activated Ag-4 (VLA-4)- vascular adhesion molecule-1 (VCAM-1) pathway plays an important role in T cell leptomeningeal recruitment(29). Given the reduction of $CD8^+$ T cell trafficking to meninges, we evaluated VLA-4 levels in meningeal and dCLN $CD8^+$ T cells by flow cytometric analysis. We observed that VLA-4 levels in $CD8^+$ T cells from both leptomeningeal space and those from dCLNs were downregulated in mice injected with LM-phenotype cells, compared with those of mice injected with parental cells (Figure 5B—figure supplement 5B). Similar results were found in BALB/c mice injected with 4T1 parental and LM cells (Figure supplement 5C). To evaluate the function of VLA-4 in breast cancer leptomeningeal metastasis, we applied neutralizing antibody against VLA-4 and found that VLA-4 blockade decreased the number of $CD8^+$ T cell in meninges (Figure 5C), and aggregated intracranial tumor metastasis, determined by histopathology (Figure 5D) and BLI signaling (Figure 5E-F).

To further investigate the role of VLA-4 in T cell trafficking, we have examined the contribution of VLA-4 in the adhesion and migration of $CD8^+$ T cells. LM- or Parental-$CD8^+$ T cells were isolated from dCLNs and tested for their ability to adhere to plate-bound VCAM-1-Ig fusion protein (Figure 5G) (3). Parental-$CD8^+$ T cells with higher expression of VLA-4 exhibited specific adhesion to plate-bound VCAM-1-Ig (74.77±4.27%), whereas, LM- $CD8^+$ T cells with lower expression of VLA-4 displayed only background levels of adhesion (9.96±0.89%). Pretreatment of Parental-$CD8^+$ T cells with the anti-VLA-4 Ab virtually ablated their ability to adhere to VCAM-1(19.22±3.44%), while LM-$CD8^+$ T cells pretreated with the anti-VLA-4 Ab showed

no difference in their ability to adhere to VCAM-1 (8.43±0.85%)(Figure 5G). To investigate the role of VLA-4 in T cell migration, we employed an *in vitro* blood-brain barrier model to assess the transmigration of T cells. Briefly, primary glial cell cultures were obtained from newborn mouse cerebral cortex and the capillaries were isolated from arterioles and venules of the brain vascular components. The digested capillaries were directly plated on the upper side of matrigel-coated inserts. Filters were placed in multi-well dishes containing stabilized glial cell cultures. Under such conditions, endothelial cells (ECs) migrated from digested capillaries and reached confluence about 4–5 days after plating. $CD8^+$ T cells were added to the top chamber and treated with IgG or VLA4 antibody. We observed that the migration of Parental-$CD8^+$ T cells was much stronger than LM-$CD8^+$ T cells, which was disrupted by anti-VLA4 treatment (Figure 5H). Furthermore, VLA-4 blockade had no effect on the proliferation (Figure 5I—figure supplement 5D) and cell death (Figure 5J—figure supplement 5E) of dCLN $CD8^+$ T cells. Taken together, these data suggested that blocking VLA-4 in $CD8^+$ T cells inhibited their adhesion and migration, leading to the impaired recruitment to meninges and lack of the capacity to control leptomeningeal metastasis.

**VLA-4 transcription is repressed by p53**

To further explore the mechanisms for VLA-4 downregulation in LM-$CD8^+$ T cells, we predicted the possible transcription factors that binding to VLA-4 promoter by three different algorithms (JASPAR, PROMO, and TFBIND). Interestingly, we found p53, the senescence marker, which functions as a transcription factor involved in a myriad of cellular activities (30). To explore whether VLA-4 transcription is controlled by p53 signaling, we examined the VLA-4 expression in the $CD8^+$ T cells isolated from dCLNs of wild type (WT) and p53-deficient (*Trp53*$^{-/-}$) mice injected with LM-phenotype cells. We found that VLA-4 levels in dCLN $CD8^+$ T cells were lower in WT mice injected with LM-EO771 cells. By comparison, p53 knockout restored VLA-4 levels of $CD8^+$ T cells in *Trp53*$^{-/-}$ mice inoculated with LM-EO771 cells(Figure 6A), suggesting that p53 mediated VLA-4 suppression in $CD8^+$ T cells. In silico analyses performed with

three different algorithms (JASPAR, PROMO, and TFBIND) predicted one putative p53-binding site located at -1550 to -1525bp upstream of the VLA-4(*Itga4*) transcription start site (TSS) (Figure 6B). We electronically transfected pGL3 reporter plasmids containing the wild type or mutant luciferase constructs of p53-binding sites of 5'-flanking region upstream of *Itga4* into EL4 lymphoma cells, a T lymphoma cell line previously used for gene transcription studies(31). Upon p53 forced expression, the luciferase signal of EL4 cells transfected with full length *Itga4* TSS decreased. Moreover, mutation of p53-binding site abolished the suppression of luciferase activity (Figure 6C). To confirm these results in an endogenous setting, we performed chromatin immunoprecipitation (ChIP)–qPCR with an antibody against p53 and found an average 4.26-fold enrichment was obtained with anti-p53 antibody in the LM-$CD8^+$ T cells, as compared to ChIP with a control immunoglobulin G (IgG). By contrast, an average 1.03-fold enrichment was found in Parental-$CD8^+$ T cells (Figure 6D). To further illustrate the contribution of p53 in leptomeningeal metastasis, we injected LM-phenotype or parental tumor cells in wild type and *Trp53*$^{-/-}$ mice. In *Trp53*$^{-/-}$ mice, the senescence of $CD8^+$ T cells was prevented as a result of p53 deficiency (Figure supplement 6A-B), contributing to upregulation of VLA-4 (Figure 6A) and enhanced trafficking ability to meninges (Figure supplement 6C-D). Therefore, tumor growth was inhibited in P53 deficient mice determined by BLI signal (Figure supplement 6E-F). Taken together, these results demonstrated that VLA-4 transcription in T cells in leptomeningeal metastasis is suppressed by the senescence factor p53.

**Meningeal $CD8^+$ T cells exhibit VLA-4 downregulation and senescence in human leptomeningeal metastasis**

To evaluate whether this finding in the animal model is consistent with patients with leptomeningeal metastasis, we investigated VLA-4 expression and the senescence phenotype in human T cells isolated from CSF of 145 patients with non-malignant neurological diseases and 45 patients with leptomeningeal involvements, including 6 cases of breast cancer, 35 cases of lung cancer, and 4 cases of gastrointestinal cancer

(Figure 7A). We found that the proportion of SA-β-gal$^+$CD8$^+$ T cells was higher in CSF from metastatic patients, compared with those of non-malignant neurological disease patients (Figure 7B—figure supplement 7A), indicating that intracranial CD8$^+$ T cells experienced senescence in patients with leptomeningeal metastasis. Moreover, flow cytometry analysis showed the CSF CD8$^+$ T cells of metastatic patients had lower expression of VLA-4 (Figure 7C). Moreover, the percentage of SA-β-gal$^+$CD8$^+$ T cells was negatively correlated with VLA-4 levels in CD8$^+$ T cells of LM patients (Figure 7D). Collectively, these results indicated the downregulation of VLA-4 and senescence in CD8$^+$ T cells in leptomeningeal metastasis (Figure 7E).

## Materials and Methods

### Mice

Six-eight-week-old female C57BL/6 mice, BALB/c mice, nude mice were purchased from the Laboratory Animal Center of Sun Yat-Sen University. *Rag2*$^{-/-}$ mice[B6(Cg)-Rag2$^{tm1.1Cgn}$/J, 008449] were purchased from the Jackson Laboratory. *Trp53*$^{-/-}$ mice, OT-1 mice on a fully C57BL/6 background were obtained from Shanghai Model Organisms Center Inc (Shanghai, China). All mice were bred and maintained in the specific-pathogen-free (SPF) animal facility of the Laboratory Animal Center of Sun Yat-Sen University. Mice were randomized at the beginning of each experiment and experiments were not blinded. All procedures were approved by the Animal Care and Use Committee of Sun Yat-Sen University.

### Cell culture and treatment

The murine breast cancer cell lines, EO771 cells were obtained from CH3 Biosystems (New York, USA). Murine 4T1, Lewis Lung Cancer (LLC) cell lines were purchased from ATCC. All the cells and their derivatives were cultured in DMEM or RPIM 1640 with 10% fetal bovine serum (FBS), 2 mM L-glutamine and 100 units/mL penicillin-streptomycin (all from GIBCO). All the cell lines were tested negative for mycoplasma contamination. EO771, 4T1 and LLC cells were forced expressed with firefly luciferase.

EO771 cells were transduced with the viral vectors of ovalbumin (EO771-OVA, GenePharma) or glycoprotein B (EO771-gB, Guangzhou Ige Biotechnology) (multiplicity of infection[MOI] of 10) overnight at 37℃ with 5 μg/mL polybrene (GenePharma). The established cells were selected by 2 μg/mL puromycin (Sigma).

**Establishment of leptomeningeal metastasis model**

A leptomeningeal metastasis model was generated as previously described with modifications(32-34). For establishing breast cancer leptomeningeal metastasis model, leptomeningeal derivative cell line was selected and injected intracardially into C57BL/6 mice. In detail, $2\times10^4$ EO771 cells, $2\times10^4$ 4T1 cells and $2\times10^4$ LLC cells transduced with lentivirus with forced expression of firefly luciferase (GenePharma) were suspended in 10 μL of PBS and then injected into the cisterna magna of recipient mice. Tumor burdens were monitored by Bioluminescent (BLI). Mice were sacrificed when leptomeningeal metastases were detected by BLI, or the clinical signs of brain metastasis, including primary central nervous system disturbances, weight loss, and behavioral abnormalities, were shown. Then, tumor cells were collected from meninges, selected by puromycin and re-injected to the second recipient mice. The operations described above were repeated three times to derivate intermediate cell line which could survive within the cerebrospinal fluid (CSF). $1\times10^5$ intermediate EO771-luc, 4T1-luc or LLC-luc cells were inoculated into the intracarotid artery of mice. After leptomeningeal metastases were detected, mice were sacrificed and tumor cells from meninges were isolated and cultured *in vitro* which were identified as LM-phenotype cell line. $1\times10^5$ LM-phenotype cells were injected into intracarotid artery of mice to establish the leptomeningeal metastasis model and tumor burden was monitored by BLI and MRI.

**IVIS Lumina imaging**

Formation of leptomeningeal metastases were monitored by IVIS Lumina imaging. Before imaging, mice were anesthetized with ketamine/xylazine injection and injected

with d-luciferin (300mg/kg). After ten minutes, mice were imaged with Xenogen IVIS Lumina system (Caliper Life Sciences). Images were analyzed by Living Image software v.3.0. (Caliper Life Sciences) and BLI flux (photons/s/cm$^2$/steradian) was calculated.

**MRI imaging**

MRI experiments were performed on Aspect M3 (1.05 Tesla, Aspect Imaging). Animals were anesthetized with ketamine/xylazine injection throughout the imaging procedure. T1 weighted SE images (TR = 0.6 sec; TE = 23 ms) were taken with or without a bolus of 0.5 mmol/kg Gd-DTPA(intravenously, 12.5 min in circulation)(35).

**Immunofluorescence and immunohistochemistry**

Paraffin-embedded samples were sectioned at 4μm thickness. Sections were de-paraffinized, rehydrated and boiled in a pressure cooker for 2 min in 10 mM citrate buffer (pH 6.0) for antigen retrieval. Then sections were blocked in PBS containing 5% bovine serum albumin (BSA) for 15 min at room temperature. For immunofluorescence assay, sections were incubated with primary antibodies specific for firefly luciferase (Abcam, Cat.No. ab185924, 1:100) overnight at 4℃ and subsequently incubated with Alexa Fluor-488, 555 or 647 conjugated secondary antibodies (Thermo Fisher Scientific, Cat.No. A32731, A32727, A-21247, 1:300) for 1 h at room temperature. Cells were counterstained with DAPI. Images were obtained by laser scanning confocal microscopy. For immunohistochemistry assay, sections were incubated with antibodies specific for luciferase (Abcam, Cat.No. ab185924, 1:100) overnight at 4℃. The immunodetection was performed using DAB (Dako) according to the manufacturer's instructions.

**Transcriptomic Analysis**

Cells cultured in T25 flask at 75% confluency were collected in TRIzol Reagent (Invitrogen) for RNA extraction. mRNA purified from cancer cells was used for library

construction with TruSeq RNA Sample Prep Kit v2 (Illumina) following the manufacturer's instructions. Samples were barcoded and run on a Hiseq 2000 platform in a 50bp/50bp paired-end run, using the TruSeq SBS Kit v3 (Illumina). An average of 40 million paired reads were generated per sample. FASTQ files from RNA-Seq results were quality assessed by FastQC v0.11.3. Raw reads were mapped to human genome hg19 (GRCh37, Feb 2009) or mouse genome mm10 (GRCm38, Dec 2011) using STAR2.3.0e(36) with standard settings for paired-end sequencing reads. In average 84% of raw reads were uniquely mapped. Mapped reads were counted to each gene by HTSeq v0.5.4with default settings. Differential gene expression analysis were performed following the instructions of "DESeq2" package deposited in Bioconductor.

**_In vivo_ administration of antibodies**

Depleting antibodies to CD4 [GK1.5] and CD8 [53.6.72] were administered by intraperitoneal injection (0.25 mg/mouse) on day 1, 4 and 6. Blocking antibody to VLA-4[PS/2] was administered by intraperitoneal injection (0.25 mg/ mouse) on day 0, 1, 2 since the day of tumor cell injection. Rat-anti-mouse IgG (Cat.No. BE0090) was used as control antibody. All antibodies were obtained from BioXCell.

**Evans blue injection and detection**

Mice were anesthetized by ketamine/xylazine intraperitoneal (i.p.) injection, and then 5μl of 10% Evans blue (Sigma-Aldrich) was delivered into the cisterna magna via intracerebroventricular (i.c.v) injection. Thirty minutes after injection, the CNS draining lymph nodes were dissected for assessment of Evans blue.

**Isolation of immune cells from secondary lymphoid organs**

Briefly, mice were anesthetized with ketamine/xylazine injection. Spleen, inguinal lymph nodes or dCLNs were isolated, smashed and filtered through a 40 μm filter to obtain single-cell suspension. For acquisition of meninge immune cells, transcardial perfusion with 30 mL of PBS via intracardiac puncture was performed before meninge

isolation(9).

**Adoptive T cell transfer**

For adoptive T cell transfer therapy, dCLNs from mice injected with EO771-luc cells were smashed and filtered through a 40 μm filter to obtain single-cell suspension. $CD4^+$ and $CD8^+$ T cells were purified by magnetic-activated cell sorting (Miltenyi, Cat.No. 130-117-043, 130-096-495). Cell populations were confirmed to be > 90% pure by flow cytometric analysis. Thereafter, $5\times10^5$ $CD4^+$ and $CD8^+$ T cells were injected into *Rag2*$^{-/-}$ mice via caudal veins, respectively.

**Flow cytometry**

Cells collected from secondary lymph organs or cerebrospinal fluid of patients were stained with fluorescent-conjugated antibody: fixable viability dye (Thermo Fisher Scientific, Cat.No. 65-0866-14), CD45 (Biolegend, Cat. No. 103132), CD3 (Biolegend, Cat.No. 100213), CD8 (Thermo Fisher Scientific, Cat.No. 53-0081-82, 17-0088-42), CD4 (Thermo Fisher Scientific, Cat.No. 62-00420-80), CD11b(Biolegend, Cat. No.101222), Ly6G(Biolegend, Cat. No. 127613), Ly6C(Biolegend, Cat. No.128017) CD11c (Biolegend, Cat.No. 117322), H-2Kb bound to SIINFEKL(Biolegend, Cat. No.141605) OVA pentamer (ProImmune, Cat.No. F93-2A-G), SA-β-gal (Dojindo, Cat.No. SG03), and CD49d (Thermo Fisher Scientific, Cat.No. 12-0492-81, 16-0492-85) for 30 min at 4°C; primary antibodies: luciferase (Abcam, Cat.No. ab185924, 1:100), cleaved caspase-3(Cell Signaling Technology, Cat.No. 9661, 1:200), Ki-67(Thermo Fisher Scientific, Cat.No. 14-5698-80, 1:50). For intracellular staining, cells were pretreated with Foxp3/Transcription Factor Fixation/Permeabilization Concentrate and Diluent (eBioscience, Cat.No. 00-5521-00) according to the manufacturer's instructions. Flow cytometry was performed on Attune NxT Flow Cytometer (Thermo Fisher Scientific) and analyzed using FlowJo software.

***Ex vivo* activation of T cells**

PBS, EO771 and EO771-gB and EO771-OVA were injected into C57BL/6 mice via cisterna magna. 7 days after tumor cell injection, DCs were isolated from murine lymph nodes using magnetic beads according to the manufacturer's instructions (Miltenyi Biotec, Cat.No. 130-100-875). OT-1 T cells were isolated from peripheral blood of OT-1 mice and labeled with 0.5μM CFSE (Thermo Fisher, Cat.lot. C34554) for 15 min at 37℃. After purification, DCs cells ($5 \times 10^4$) and CFSE-labeled OT-1 T cells ($10^5$) were incubated in flat 96-well plate for 60 hours. Subsequently, OT-1 T cells were harvested for flow cytometry analysis and IFN-γ ELISpot assay.

**IFN-γ ELISpot assay**

ELISpot assays were performed using a mouse IFN-γ ELISpot kit according to the manufacturer's procedure (DAKAWE, China). The harvested OT-1 T cells were added to ELISpot plates and cultured overnight at 37℃. Plates were then washed 4 times with washing buffer, and incubated with biotinylated detection antibody for IFN-γ (DAKAWE, China) for 1 h at 37 °C. Following 4 additional washes with washing buffer, the plates were incubated with avidin–horseradish peroxidase (HRP) (DAKAWE, China) for 1 h at 37 °C. Plates were then washed 4 more times with washing buffer and 2 washes with PBS. After 15 min incubation with AEC substrate (BD), the reaction was stopped. The plates were washed with deionized water and dried overnight before membrane removal. Spots were counted using an ELISpot reader (ImmunoSpot S6 ULTRA-V, Cellular Technology, Cleveland, OH).

**Lymphatic vessel ligation**

Mice were anaesthetized by i.p. injection with ketamine and xylazine in saline, the skin of the neck was shaved and cleaned with iodine and 70% ethanol. A midline incision was made 5 mm superior to the clavicle. The sternocleidomastoid muscles were retracted and the dCLNs were exposed on each side. Ligation of the afferent lymphatic vessels on each side was performed with 10-0 synthetic, non-absorbable sutures. Control mice were subjected to a sham surgery consisting of the skin incision and

retraction of the sternocleidomastoid muscle only. The skin was then sutured and allowed to recover on a heat pad until fully awake.

**Two-photon microscopy**

Before two-photon microscopy, $1\times10^6$ $CD8^+$ T cells from dCLNs of mice injected with parental or LM cells were isolated, labeled by 0.5 μM CFSE (Thermo Fisher, Cat.lot. C34554) for 15 min at 37℃, and transferred to recipient mice via caudal veins. 24 h after T cell transfusion, mice were anesthetized, and thinned skull windows were prepared. Mice were injected with 100 μL rhodamine dextran solution (100mg/mL, Sigma, R9379) where indicated to visualize blood vessels. Images were captured in z-stacks of 10–30 planes (1 μm step size) using an Olympus FVMPE-RS two-photon microscope.

**Whole mount meninge preparation**

Anesthetized mice were euthanized, brains were sterilely dissected and placed in ice-cold sterile PBS. Meninges within the skullcap were fixed in 4% paraformaldehyde (PFA) overnight, and separated from the skullcap. Then the meninges were incubated in the block-perm buffer containing 2% normal goat serum, 1% BSA , 0.1% Triton X and 0.05% Tween for 1 h at room temperature with gentle rocking. The primary antibody anti-mouse CD8 (Novus, Cat.No. ABX-160A, 1:100), anti-lyve-1 (R&D Systems, Cat.No. AF2125) and the secondary antibody Alexa Fluor 488, 555 rabbit anti-mouse IgG, Alexa Fluor 555 rabbit anti-goat IgG (Life Technologies) were employed for $CD8^+$ T cell and lymphatic vessel staining. The meninges were mounted with Prolong Gold with DAPI (Molecular Probes).

**DTCs detection with luciferase assay**

100 μL blood was centrifuged at 92 × g for 5 min, and plasma was discarded. Cell lysis buffer (200 μL) (Beyotime Biotechnology Co., Ltd.) was added to resuspend cells, incubated at room temperature for 8-10 min with occasional shaking, then centrifuged

at 12,000 × g for 5 min. The supernatant was aspirated into another tube and the sediment were subsequently for flow cytometry and luciferase assay. For flow cytometry, cells were stained with anti-firefly luciferase (Abcam, Cat.No. ab185924, 1:100) and anti-CD45 antibodies(Biolegend, Cat. No. 103132). For luciferase assay, 100 μL of luciferin working solution (Beyotime Biotechnology Co., Ltd.) was added to the sample, reacting with luciferase of DTCs of EO771-luc. Immediately, the RLU in each sample was assayed by luminometer (Infinite M200 Pro, Tecan). To set up standard curve, the freshly harvested Luc-EO771 cells were counted, then 0, 5, 10, 20, 30, 40, 50, 60 cells were added to tubes, respectively. RLU was assayed according to the above method and the derived equation was used as standard curve to calculate the DTC numbers of Luc-EO771 cells from mice with metastases.

**Cell adhesion assays**

96-well-ELISA plates were coated with 10 μg/ml of mouse VCAM-1-Ig or heat-denatured BSA. T cells were harvested and suspended in binding buffer (0.5% BSA, 2 mM $CaCl_2$, 2 mM $MgCl_2$ in PBS), and then added to the plate. For blocking experiments, cells resuspended in binding buffer were pretreated with 20 μg/ml of anti-CD49d mAbs (PS/2) for 15 min at 37°C, and then added to the plate. Plates were centrifuged at 500 rpm for 1 min and cells were allowed to adhere for 30 min at room temperature with gentle shaking. The plate was then gently washed three times using binding buffer and the number of adherent cells were enumerated by flow cytometry. Percent adhesion was calculated as the (number of adherent cells to VCAM-1-Ig - number of adherent cells to heat-denatured BSA)/Number of total input cells.

**Cell migration assays**

Murine brain microvascular endothelial cells (MBMECs) were isolated as previously described(37,38). In brief, mice were sacrificed and meninge-free forebrains were collected, minced, then digested with 10 mg/mL of collagenase II and 1 mg/mL DNase(Worthington Biochemical) in DMEM in a shaker for 1 h at 37 °C. The digested

tissues were suspended with 20% bovine serum albumin solution prepared in DMEM to remove myelin. The pellets were further digested in the presence of 1 mg/ml of collagenase/dispase (Roche Applied Science) and 1 mg/mL DNase in DMEM for 1 h at 37 °C. The microvessel fragments obtained from the enzyme-digested pellets were separated on a 33% continuous Percoll gradient (700 g, 10 min), collected, and washed twice in DMEM and cultured in endothelial cell medium. Five days after isolation, MBMECs were trypsinized, resuspended in MBMEC medium, and seeded onto precoated Transwell inserts (pore size 3 μm; Corning) at $2 \times 10^4$ cells per insert. When MBMECs reached confluence, $2 \times 10^5$ T cells per insert were added directly on top of MBMECs. After 24 h, migrated cells were collected from the basolateral compartment, while non-migrating cells were recovered from the upper compartment.

**Western blot**

dCLN $CD8^+$ T cells were washed with PBS and lysed with RIPA buffer containing proteinase inhibitor. Lysates were centrifuged for 25 min at 4℃ at 12000g. Protein extracted from the cells were fractionated by 10% SDS–polyacrylamide gels and further transferred to polyvinylidene difluoride membranes. Membranes were blocked with TBS/0.05% Tween-20/5% skim milk and then incubated with primary antibodies against p53 (Proteintech, Cat.No. 10442-1-AP, 1:1000), p21 (Proteintech, Cat.No. 27296-1-AP, 1:1000) and GAPDH (Proteintech, Cat.No. HRP-60004, 1:10000) at 4℃ overnight. Membranes were washed 3 times with TBST and then incubated with peroxidase-conjugated secondary antibody (Cell Signaling Technology, Cat.No. 7074S, 1:3000). The antigen-antibody reaction was visualized by enhanced chemiluminescence assay (ECL, Thermo Fisher Scientific).

**Cellular senescence assay**

For Senescence-associated β-Galactosidase(SA-β-gal) staining, dCLN $CD8^+$ T cells were isolated, fixed, and stained for SA-β-gal at 37℃ overnight by Senescence-associated β-Galactosidase Staining Kit (Beyotime, Cat.No. C0602) according to the

599 manufacturer's instruction. For quantification of SA-β-gal-positive cells, images were
600 randomly taken at 40× magnification (BX-63, Olympus) and then analyzed manually
601 with ImageJ.
602
603 **Luciferase reporter assay**
604 The luciferase assay was performed using reporter lysis buffer and luciferase assay
605 reagent according to the manufacturer's instructions. Briefly, a fragment spanning from
606 -2000 to +100 relative to the TSS of the murine VLA-4 genomic sequence was fused
607 to pGL3-Basic vector to generate VLA-4 wild type (WT) (-2000/+100)-luc. The C/G
608 to A/T mutations at the consensus p53-binding site were introduced by site-directed
609 mutagenesis (from 5'-GGAGCCC-3' to 5'-GGATAAA-3'). For luciferase reporter
610 experiments, a murine T lymphoma cell line EL4 was transfected with VLA-4-wild
611 type-luc or VLA-4-mutant-luc reporter and pRL-TK-Renilla for 24h using a Bio-Rad
612 Gene Pilser Xcell Electroporation System. Afterwards, the cells were transduced with
613 lentivirus with p53 overexpression or empty vector. After 24h transfection, cells were
614 lysed and analyzed with the Dual-Luciferase reporter assay system (Promega, Cat.No.
615 E1960). Renilla Luciferase (R-luc) was used to normalize firefly luciferase (F-luc)
616 activity to evaluate reporter translation efficiency.
617
618 **Chromatin Immunoprecipitation Assay (ChIP)**
619 The ChIP assay was performed using a ChIP Assay Kit (Millipore) according to the
620 manufacturer's instructions. Briefly, dCLN $CD8^+$ T cells were isolated and fixed in 1%
621 formaldehyde for 10 min at room temperature. Fixed cells were washed and then lysed
622 in ChIP lysis buffer. The whole cell extracts were then sonicated for 10 cycles of 10 s
623 on /20 s off and 50% AMPL with Sonics VCX130 (Sonics & Materials, Inc, Newtown).
624 Antibodies directed against p53 (Proteintech, 10442-1-AP, 1μg) or rabbit IgG
625 (Proteintech, Cat.No. B900610, 1μg) were used. The precipitated DNA was subjected
626 to PCR amplification. The primer sequences used in ChIP assays:
627 *Itga4*: forward (5'>3') TCTTCTCAGAGTGTGTGGA;

*Itga4*: reverse (5'>3') GAGCACCCAGCAACATTT.

*Gapdh*: forward (5'>3') GCCCTGCTTATCCAGTCCTA ;

*Gapdh*: reverse (5'>3') GGTCCAAAGAGAGGGAGGAG .

*Cdkn1a*: forward (5'>3') TAGCTTTCTGGCCTTCAGGA;

*Cdkn1a*: reverse (5'>3') TGGGTATCATCAGGTCTCCA.

**Patients and tissue samples**

CSF samples were obtained from 145 cases of non-malignant neurological diseases (45 cases from brain injury, 25 cases from neurodegenerative diseases, 50 cases from cerebrovascular diseases and 25 cases from benign primary tumors) and 45 cases of brain metastasis, including 6 cases of breast cancer, 35 cases of lung cancer, and 4 cases of gastrointestinal cancer at Sun Yat-Sen Memorial Hospital, Sun Yat-Sen University (Guangzhou, China) between 2017 and 2020. CSF sample were centrifuged at 450g for 8 min, and the cells of the CSF sediment were collected for future flow cytometry analysis. To minimize bias, samples were blinded to laboratory personnel. All samples were collected from patients who had provided informed consent, and all related procedures were performed with the approval of the internal review and ethics board of Sun Yat-Sen Memorial Hospital.

**Statistics**

The number of events and information about the statistical details and methods are indicated in the relevant figure legends. Data are expressed as the mean ±SD and were analyzed using GraphPad Prism 8.0. Two-tailed Student t-tests were used to identify significant differences between two groups. One-way ANOVA with Tukey's multiple comparison test were used for comparison of more than 2 groups. Pearson's correlation was used to assess the relationship between VLA-4 expression and the activity of SA-β-gal in $CD8^+$ T cells in the CSF of patients with brain metastases. Kaplan-Meier survival curves were plotted and log-rank test was done. $P < 0.05$ was considered statistically significant.

## Discussion

Extracranial immune cells were traditionally believed to be absent in the normal CNS due to the blood–brain barrier. The recent identification of functional lymphatic vessels in brain has shifted the paradigm from immunologic privilege to a distinct immune response in CNS diseases(9,39,40). Leptomeningeal metastasis is associated with one of the worst clinical outcomes of malignancies. However, very little is known about the immune response to leptomeningeal metastasis(3). Here, we uncovered that tumor-specific $CD8^+$ T cells are generated in dCLNs and play a central role in controlling leptomeningeal metastasis. Moreover, inducing immunosenescence of $CD8^+$ T cells is essential for tumor cells to escape meningeal immune defenses and successfully establish clinical lesions in the leptomeningeal space.

During inflammation, apart from TCR signaling, T cells can also be activated in a T cell receptor-independent and cytokine-dependent manner, which is called “bystander effect”(41). Recent findings have revealed the presence of a functional lymphatic system located in the meninges(42). In the immunocompetent mouse model of breast cancer leptomeningeal metastasis that we constructed, we provided clear evidences that tumor-specific $CD8^+$ T cells can be generated in dCLNs and recruited to leptomeninges by VLA-4. T cells in dCLNs of mice bearing EO771-OVA leptomeningeal metastasis showed specific response to OVA. In addition, OVA-specific T cells undergo Ag-specific activation and proliferation *in vitro* in response to EO771-OVA injection, indicating dCLNs generate tumor-specific $CD8^+$ T cells against leptomeningeal metastasis, but not “bystander activation”. Consistent with our results, previous studies have shown that activation of CNS-specific T cells in cervical lymph nodes have a direct role in mediating the neuroinflammation observed in experimental autoimmune encephalomyelitis (EAE) (43). Therefore, our data indicated that the tumor-specific $CD8^+$ T cells primed in dCLNs play an important role in controlling leptomeningeal metastasis.

In brain tumors such as glioblastoma and brain metastases, T cells that do successfully infiltrate are subject to further suppressive influences geared at promoting such dysfunction as tolerance and exhaustion(44,45). Emerging evidences suggest that immunosenescence, which is distinct from exhaustion, is an important state of T cell dysfunction and responsible for immunosuppression in the tumor microenvironment(46). In recent studies, T cells undergo senescence in the normal aging process or in the patients with under chronic infections and cancers (47).T cell senescence has also been found to be strongly induced in several types of malignancies, including lung cancer,(48) ovarian cancer(49) and melanoma(50), through MAPK signaling (51). MAPK/p38 signaling is essential for activating the cell cycle regulatory molecules p53, p21, and p16, which might inhibit cell cycle progression to slow or completely arrest DNA replication and induce cell senescence (28). However, whether senescence contributes to immunosuppression in CNS metastasis remained elusive. In our study, we found that T cells in dCLNs from leptomeningeal metastatic mice exhibited senescent features, including elevated expression of p53 and p21, and increased levels of secreted senescence-associated beta-galactosidase. Previous studies have indicated that increased senescent T cells resulted in T cell proliferation arrest and killing capacity defect(52,53). Here, we advanced this emerging concept by showing that the recruitment of T cells to meninges is impaired as a result of the suppression of VLA-4. VLA-4(α4β1) is responsible for CNS tropism of T cells and VLA-4 neutralization can inhibit the homing and infiltration of antigen-specific T cells in cerebral autoimmune models(54,55). VLA-4 blockade in WT mice impedes T cell trafficking to meningeal lymphatics and aggravates leptomeningeal metastasis. Collectively, T cell senescence impairs the trafficking of T cells, leading to the failure of tumor control.

Previous studies have demonstrated that induction of p53 is pivotal for the establishment of senescence, mainly following its activation by the DNA damage

response (DDR) caused by telomere attrition, oxidative or oncogenic stress (56,57). Also, several p53-targets and regulators have been linked to induction of senescence (58). In our study, we identified a specific p53 binding site within the *Itga4* promoter, and found that the mutation of specific p53 binding site relieved its repression on the VLA-4 transcription. Consistently, in *Trp53*$^{-/-}$ mice, the senescence of CD8$^{+}$ T cells was inhibited as a result of p53 deficiency, leading to upregulation of VLA-4 and enhanced trafficking ability to meninges. Therefore, p53 deficient T cells can efficiently inhibit tumor growth, compared with wild type T cells. In addition, in line with our study, previous studies showed that p53 deficient T cells exhibited decreased apoptosis (59) and enhanced proliferation in T cells(60), supporting that p53 deficient T cells have higher anti-tumor effector function.

Collectively, our findings revealed that tumor-specific immunity originated from draining dCLNs is essential for restraining leptomeningeal metastasis. Senescence signals inhibit trafficking of CD8$^{+}$ T cells from dCLNs to meninges and therefore promote the progression of leptomeningeal metastasis.

**Additional information**

Funding: This work was supported by grants from the National Key Research and Development Program of China (2021YFA1300502), the Natural Science Foundation of China (91942309, 92057210, 82222029, 81802643, 82071754, 81971481, 82002786, 82003859), the Natural Science Foundation of Guangdong Province (2018A030310085, 2020A1515011458, 2018A030313769, 2019A1515011632, 2021A1515010230), Science and Technology Program of Guangzhou(202103000070). Guangdong Science and Technology Department (2017B030314026), Sun Yat-Sen Projects for Clinical Trials (SYS-C-202003).

Author contributions: J.L., D.H., S.S., and Y.W. conceived the ideas, designed the experiments and wrote the manuscript. J.L., D.H., X.L., Q.Z. and J.H. performed most of the experiments and analyzed the data. Y.W. and B.L. provided samples from

744 patients for clinical data analysis. All authors contributed to the revision of the
745 manuscript.

746

747 **Reference**

748 1. García-Gómez P, Priego N, Álvaro-Espinosa L, Valiente M. Brain Metastases Cell Partners
749 and Tumor Microenvironment. Central Nervous System Metastases: Springer; 2020. p 59-
750 71.
751 2. Valiente M, Ahluwalia MS, Boire A, Brastianos PK, Goldberg SB, Lee EQ, *et al.* The Evolving
752 Landscape of Brain Metastasis. Trends in cancer **2018**;4:176-96
753 3. Boire A, Brastianos PK, Garzia L, Valiente M. Brain metastasis. Nature reviews Cancer
754 **2020**;20:4-11
755 4. Franzoi MA, Hortobagyi GN. Leptomeningeal carcinomatosis in patients with breast
756 cancer. Critical reviews in oncology/hematology **2019**;135:85-94
757 5. Wang N, Bertalan MS, Brastianos PK. Leptomeningeal metastasis from systemic cancer:
758 Review and update on management. Cancer **2018**;124:21-35
759 6. Kushner BH, Cheung NK. Absolute requirement of CD11/CD18 adhesion molecules, FcRII
760 and the phosphatidylinositol-linked FcRIII for monoclonal antibody-mediated neutrophil
761 antihuman tumor cytotoxicity. Blood **1992**;79:1484-90
762 7. Niwińska A, Rudnicka H, Murawska M. Breast cancer leptomeningeal metastasis:
763 propensity of breast cancer subtypes for leptomeninges and the analysis of factors
764 influencing survival. Medical oncology (Northwood, London, England) **2013**;30:408
765 8. Louveau A, Smirnov I, Keyes TJ, Eccles JD, Rouhani SJ, Peske JD, *et al.* Structural and
766 functional features of central nervous system lymphatic vessels. Nature **2015**;523:337-41
767 9. Louveau A, Herz J, Alme MN, Salvador AF, Dong MQ, Viar KE, *et al.* CNS lymphatic
768 drainage and neuroinflammation are regulated by meningeal lymphatic vasculature.
769 Nature neuroscience **2018**;21:1380-91
770 10. Bartholomäus I, Kawakami N, Odoardi F, Schläger C, Miljkovic D, Ellwart JW, *et al.* Effector
771 T cell interactions with meningeal vascular structures in nascent autoimmune CNS lesions.
772 Nature **2009**;462:94-8
773 11. Schläger C, Körner H, Krueger M, Vidoli S, Haberl M, Mielke D, *et al.* Effector T-cell
774 trafficking between the leptomeninges and the cerebrospinal fluid. Nature **2016**;530:349-
775 53
776 12. Bray F, Ferlay J, Soerjomataram I, Siegel RL, Torre LA, Jemal A. Global cancer statistics
777 2018: GLOBOCAN estimates of incidence and mortality worldwide for 36 cancers in 185
778 countries. CA: a cancer journal for clinicians **2018**;68:394-424
779 13. Aunan JR, Cho WC, Søreide K. The Biology of Aging and Cancer: A Brief Overview of
780 Shared and Divergent Molecular Hallmarks. Aging and disease **2017**;8:628-42
781 14. Faget DV, Ren Q, Stewart SA. Unmasking senescence: context-dependent effects of SASP
782 in cancer. Nat Rev Cancer **2019**;19:439-53
783 15. Fane M, Weeraratna AT. How the ageing microenvironment influences tumour
784 progression. Nat Rev Cancer **2020**;20:89-106
785 16. Ye J, Ma C, Hsueh EC, Dou J, Mo W, Liu S, *et al.* TLR8 signaling enhances tumor immunity

by preventing tumor-induced T-cell senescence. EMBO molecular medicine **2014**;6:1294-311

17. Ye J, Ma C, Hsueh EC, Eickhoff CS, Zhang Y, Varvares MA*, et al.* Tumor-Derived γδ Regulatory T Cells Suppress Innate and Adaptive Immunity through the Induction of Immunosenescence. The Journal of Immunology **2013**;190:2403-14
18. Ransohoff RM, Engelhardt B. The anatomical and cellular basis of immune surveillance in the central nervous system. Nature reviews Immunology **2012**;12:623-35
19. Manglani M, Gossa S, McGavern DBJCpii. Leukocyte isolation from brain, spinal cord, and meninges for flow cytometric analysis. **2018**;121:e44
20. Fan KQ, Li YY, Wang HL, Mao XT, Guo JX, Wang F*, et al.* Stress-Induced Metabolic Disorder in Peripheral CD4(+) T Cells Leads to Anxiety-like Behavior. Cell **2019**;179:864-79.e19
21. Chandrasekaran S, King MRJIJoMS. Microenvironment of tumor-draining lymph nodes: opportunities for liposome-based targeted therapy. **2014**;15:20209-39
22. Maloveska M, Danko J, Petrovova E, Kresakova L, Vdoviakova K, Michalicova A*, et al.* Dynamics of Evans blue clearance from cerebrospinal fluid into meningeal lymphatic vessels and deep cervical lymph nodes. Neurological research **2018**;40:372-80
23. Bandola-Simon JM, Roche PA. Dendritic cells dysfunction in tumor-draining lymph nodes. The Journal of Immunology **2019**;202:135.16
24. Alfei F, Ho P-C, Lo W-LJO. DCision-making in tumors governs T cell anti-tumor immunity. **2021**;40:5253-61
25. Tavares GA, Louveau AJC. Meningeal Lymphatics: An Immune Gateway for the Central Nervous System. **2021**;10:3385
26. Kim RJCI. Cancer immunoediting: from immune surveillance to immune escape. **2007**:9-27
27. Calzascia T, Masson F, Di Berardino-Besson W, Contassot E, Wilmotte R, Aurrand-Lions M*, et al.* Homing phenotypes of tumor-specific CD8 T cells are predetermined at the tumor site by crosspresenting APCs. Immunity **2005**;22:175-84
28. Montes CL, Chapoval AI, Nelson J, Orhue V, Zhang X, Schulze DH*, et al.* Tumor-induced senescent T cells with suppressor function: a potential form of tumor immune evasion. Cancer research **2008**;68:870-9
29. Theien BE, Vanderlugt CL, Nickerson-Nutter C, Cornebise M, Scott DM, Perper SJ*, et al.* Differential effects of treatment with a small-molecule VLA-4 antagonist before and after onset of relapsing EAE. Blood **2003**;102:4464-71
30. Wang B, Xiao Z, Ren EC. Redefining the p53 response element. Proceedings of the National Academy of Sciences of the United States of America **2009**;106:14373-8
31. Kao C, Oestreich KJ, Paley MA, Crawford A, Angelosanto JM, Ali MA*, et al.* Transcription factor T-bet represses expression of the inhibitory receptor PD-1 and sustains virus-specific CD8+ T cell responses during chronic infection. Nature immunology **2011**;12:663-71
32. Boire A, Zou Y, Shieh J, Macalinao DG, Pentsova E, Massagué J. Complement Component 3 Adapts the Cerebrospinal Fluid for Leptomeningeal Metastasis. Cell **2017**;168:1101-13.e13
33. Fults DW, Taylor MD, Garzia L. Leptomeningeal dissemination: a sinister pattern of medulloblastoma growth. Journal of neurosurgery Pediatrics **2019**:1-9

34. Chi Y, Remsik J, Kiseliovas V, Derderian C, Sener U, Alghader M, *et al.* Cancer cells deploy lipocalin-2 to collect limiting iron in leptomeningeal metastasis. Science (New York, NY) **2020**;369:276-82
35. Brandsma D, Taphoorn MJ, Reijneveld JC, Nas TM, Voest EE, Nicolay K, *et al.* MR imaging of mouse leptomeningeal metastases. **2004**;68:123-30
36. Engström PG, Steijger T, Sipos B, Grant GR, Kahles A, Rätsch G, *et al.* Systematic evaluation of spliced alignment programs for RNA-seq data. **2013**;10:1185-91
37. Meena M, Van Delen M, De Laere M, Sterkens A, Costas Romero C, Berneman Z, *et al.* Transmigration across a Steady-State Blood–Brain Barrie Induces Activation of Circulating Dendritic Cells Partly Mediated by Actin Cytoskeletal Reorganization. **2021**;11:700
38. Ruck T, Bittner S, Epping L, Herrmann AM, Meuth SGJJ. Isolation of primary murine brain microvascular endothelial cells. **2014**:e52204
39. Ahn JH, Cho H, Kim JH, Kim SH, Ham JS, Park I, *et al.* Meningeal lymphatic vessels at the skull base drain cerebrospinal fluid. Nature **2019**;572:62-6
40. Forrester JV, McMenamin PG, Dando SJ. CNS infection and immune privilege. Nature reviews Neuroscience **2018**;19:655-71
41. Kim TS, Shin EC. The activation of bystander CD8(+) T cells and their roles in viral infection. Experimental & molecular medicine **2019**;51:1-9
42. Da Mesquita S, Louveau A, Vaccari A, Smirnov I, Cornelison RC, Kingsmore KM, *et al.* Functional aspects of meningeal lymphatics in ageing and Alzheimer's disease. Nature **2018**;560:185-91
43. Furtado GC, Marcondes MC, Latkowski JA, Tsai J, Wensky A, Lafaille JJ. Swift entry of myelin-specific T lymphocytes into the central nervous system in spontaneous autoimmune encephalomyelitis. Journal of immunology (Baltimore, Md : 1950) **2008**;181:4648-55
44. Farber SH, Tsvankin V, Narloch JL, Kim GJ, Salama AK, Vlahovic G, *et al.* Embracing rejection: Immunologic trends in brain metastasis. Oncoimmunology **2016**;5:e1172153
45. Woroniecka K, Chongsathidkiet P, Rhodin K, Kemeny H, Dechant C, Farber SH, *et al.* T-Cell Exhaustion Signatures Vary with Tumor Type and Are Severe in Glioblastoma. Clinical cancer research : an official journal of the American Association for Cancer Research **2018**;24:4175-86
46. Nikolich-Žugich J. Aging of the T cell compartment in mice and humans: from no naive expectations to foggy memories. Journal of immunology (Baltimore, Md : 1950) **2014**;193:2622-9
47. Zhao Y, Shao Q, Peng GJC, immunology m. Exhaustion and senescence: two crucial dysfunctional states of T cells in the tumor microenvironment. **2020**;17:27-35
48. Chen C, Chen D, Zhang Y, Chen Z, Zhu W, Zhang B, *et al.* Changes of CD4+CD25+FOXP3+ and CD8+CD28- regulatory T cells in non-small cell lung cancer patients undergoing surgery. International immunopharmacology **2014**;18:255-61
49. Wu M, Chen X, Lou J, Zhang S, Zhang X, Huang L, *et al.* Changes in regulatory T cells in patients with ovarian cancer undergoing surgery: Preliminary results. International immunopharmacology **2017**;47:244-50
50. López-Otín C, Blasco MA, Partridge L, Serrano M, Kroemer G. The hallmarks of aging. Cell **2013**;153:1194-217

51. Wang W, Chen JX, Liao R, Deng Q, Zhou JJ, Huang S*, et al.* Sequential activation of the MEK-extracellular signal-regulated kinase and MKK3/6-p38 mitogen-activated protein kinase pathways mediates oncogenic ras-induced premature senescence. Molecular and cellular biology **2002**;22:3389-403
52. Ye J, Peng G. Controlling T cell senescence in the tumor microenvironment for tumor immunotherapy. Oncoimmunology **2015**;4:e994398
53. Appay V, Nixon DF, Donahoe SM, Gillespie GM, Dong T, King A*, et al.* HIV-specific CD8(+) T cells produce antiviral cytokines but are impaired in cytolytic function. The Journal of experimental medicine **2000**;192:63-75
54. Burkly LC, Jakubowski A, Hattori M. Protection against adoptive transfer of autoimmune diabetes mediated through very late antigen-4 integrin. Diabetes **1994**;43:529-34
55. Zundler S, Fischer A, Schillinger D, Binder MT, Atreya R, Rath T*, et al.* The α4β1 Homing Pathway Is Essential for Ileal Homing of Crohn's Disease Effector T Cells In Vivo. Inflammatory bowel diseases **2017**;23:379-91
56. Mijit M, Caracciolo V, Melillo A, Amicarelli F, Giordano A. Role of p53 in the Regulation of Cellular Senescence. Biomolecules **2020**;10:420
57. Kumari R, Jat P. Mechanisms of Cellular Senescence: Cell Cycle Arrest and Senescence Associated Secretory Phenotype. Frontiers in cell and developmental biology **2021**;9:645593
58. Feng Z, Zhang C, Wu R, Hu W. Tumor suppressor p53 meets microRNAs. J Mol Cell Biol **2011**;3:44-50
59. Madapura HS, Salamon D, Wiman KG, Lain S, Klein G, Klein E*, et al.* p53 contributes to T cell homeostasis through the induction of pro-apoptotic SAP. Cell Cycle **2012**;11:4563-9
60. Banerjee A, Thyagarajan K, Chatterjee S, Chakraborty P, Kesarwani P, Soloshchenko M*, et al.* Lack of p53 Augments Antitumor Functions in Cytolytic T Cells. Cancer research **2016**;76:5229-40

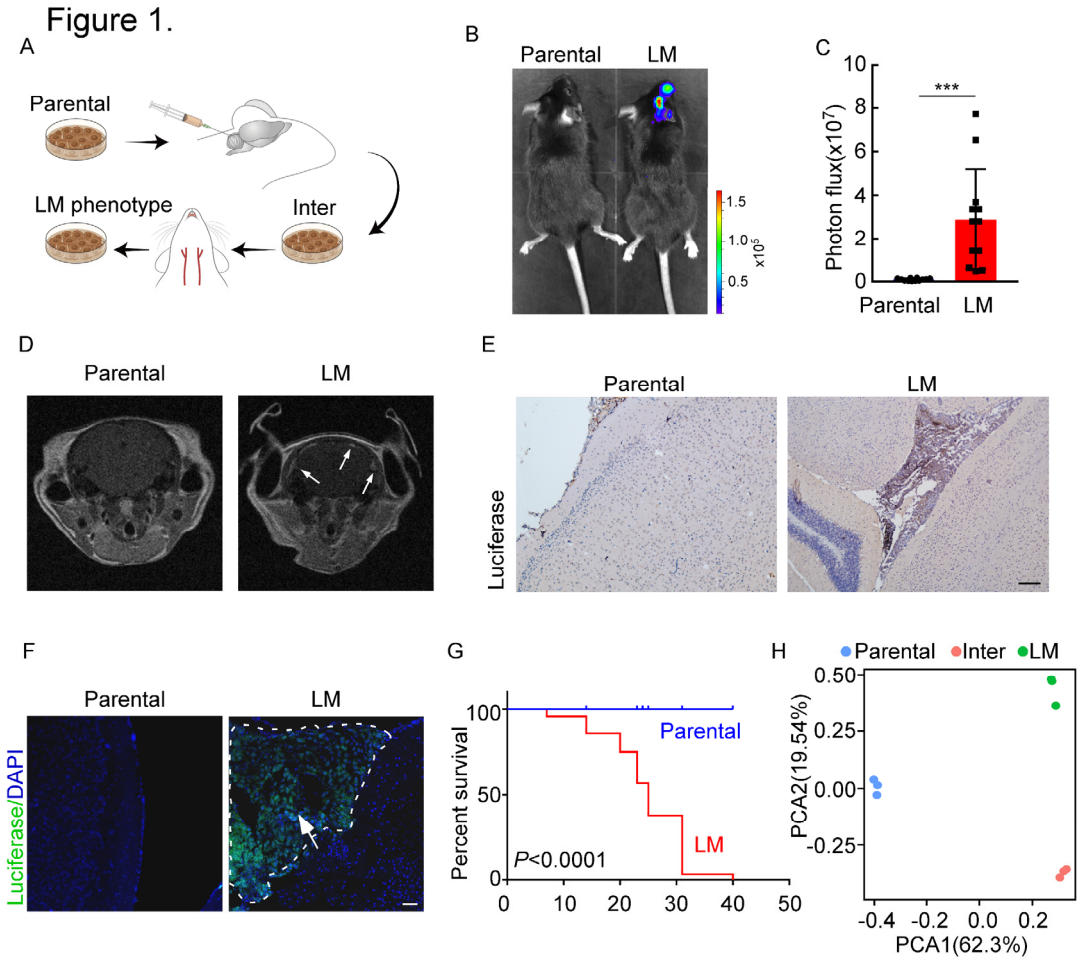


**Figure 1. Establishing a model of breast cancer leptomeningeal metastasis.**

(A) An illustration showing iterative *in vivo* selection of leptomeningeal metastatic derivative cell lines. $2\times10^4$ tumor cells transduced with lentiviral vectors expressing luciferase were injected into the cisterna magna of recipient mice. When leptomeningeal metastatic lesions were detected by IVIS, the mice were euthanized. Cells were collected and cultured before being injected into the other mice. This procedure was carried out three times to generate intermediate (Inter) cells. Next, $1\times10^5$ Inter cells were inoculated into the intracarotid artery. Mice bearing leptomeningeal metastases were sacrificed and tumor cells were collected from the meninges and denoted as LM derivatives.

(B-G) $1\times10^5$ EO771 parental or LM-phenotype cells were inoculated into the intracarotid artery of recipient mice.

(B-C) Tumor growth was monitored by BLI imaging at day 28. Representative BLI

images (B) and quantitation (C) were shown (mean ± SD, $n = 12$ mice per group.). *** $P < 0.001$ by two-tailed Student's $t$ test.

(D) MRI at day 28 post-inoculation revealed leptomeningeal metastasis was formed after LM-phenotype cell inoculation. The white arrows indicate metastatic lesions.

(E) Neuro-anatomic localization of metastases was determined by immunohistochemistry staining. Scale bar = 50μm.

(F) Representative pictures of immunofluorescence staining for leptomeningeal metastatic lesions in mice (luciferase, green; DAPI, blue). The white line indicates the border of the metastatic lesions. Scale bar = 50μm.

(G) Kaplan-Meier plot of overall survival of mice.

(H) Principal component analysis (PCA) plots of gene expression data showing a segregation among Parental (blue), LM-phenotype (green) and Inter (orange) cell lines. Genes with base mean ≥ 50, fold change ≥2 or ≤ 0.5 and $P < 0.01$ were included for analysis.

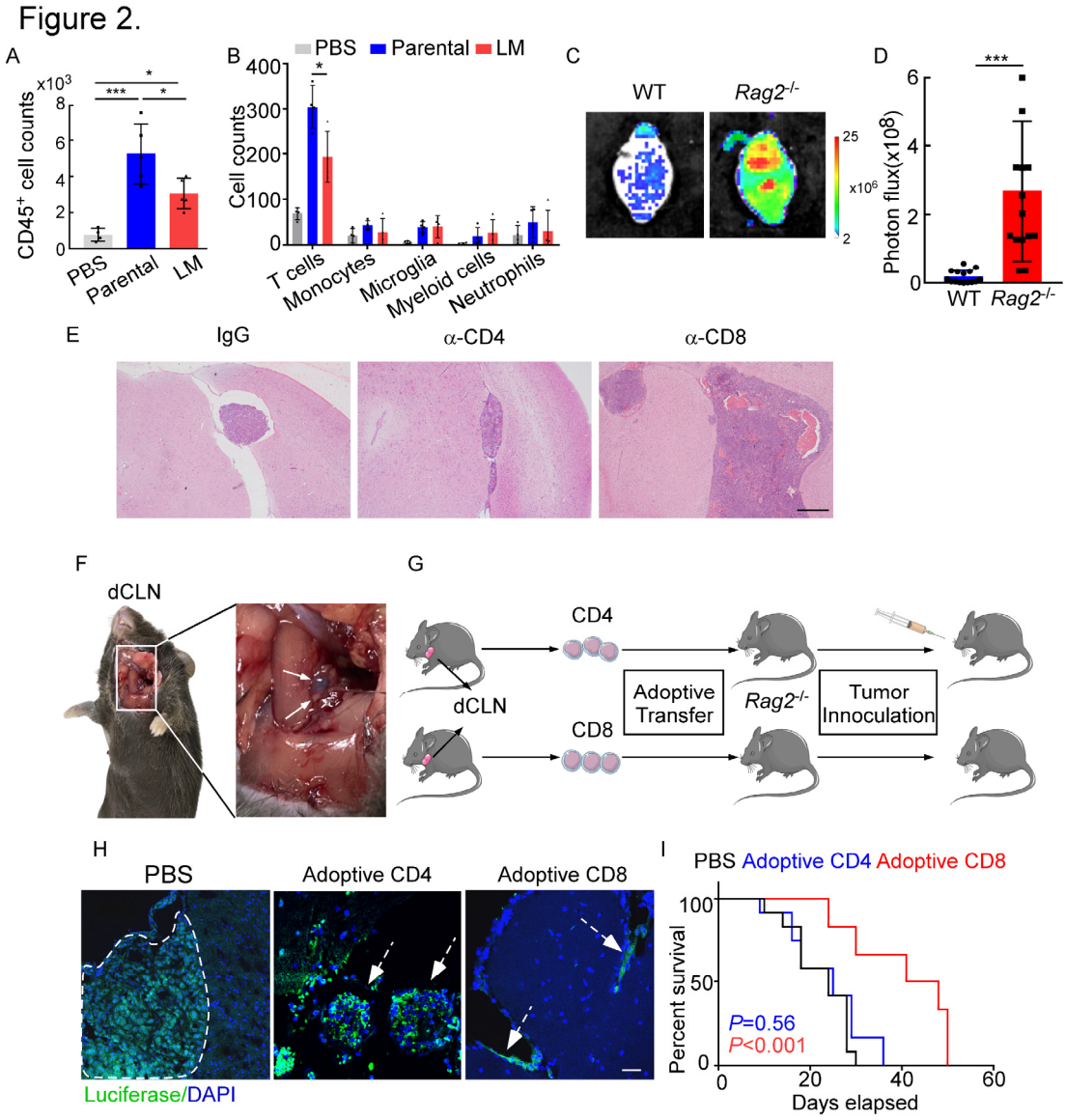


**Figure 2. CD8$^+$ T cells constrain leptomeningeal metastasis.**

(A-B) PBS, $1\times10^5$ EO771 parental or LM-phenotype cells were inoculated into the intracarotid artery of recipient mice.

(A) Histogram represents the absolute number of meningeal CD45$^+$ immune cells. (mean ± SD. PBS $n = 4$ per group; Parental, LM $n = 5$ per group.). * $P < 0.05$, *** $P < 0.001$ by one-way ANOVA with Tukey's multiple comparison test.

(B) Histogram represents the absolute number of diverse meningeal immune cells mice. (mean ± SD, $n = 4$ per group.). * $P < 0.05$ by one-way ANOVA with Tukey's multiple comparison test.

(C-D) $1\times10^5$ EO771 LM-phenotype cells were injected into the intracarotid artery of wild type C57BL/6 (WT) or *Rag2*$^{-/-}$ mice. Representative images (C) and quantitation (D) for tumor growth monitored by BLI at day 28 post-injection (mean ± SD, $n$ = 12 per group.). *** $P < 0.001$ by two-tailed Student's $t$ test.

(E) $1\times10^5$ LM-phenotype cells were inoculated into the intracarotid artery of WT C57BL/6 mice treated with IgG, anti-CD4 (α-CD4) or anti-CD8 neutralizing antibodies (α-CD8), respectively. Representative images for intracranial tumor lesions were shown ($n$ = 4 per group). Scale bar = 20μm.

(F) Evans blue was injected into the cisterna magna of WT C57BL/6 mice. The presence of dye in dCLNs was detected after 30 minutes. Representative images of the Evans blue accumulation in the dCLN. The white arrowhead points to the dCLN.

(G-I) CD4$^+$ and CD8$^+$ T cells were isolated from dCLNs of WT mice injected with EO771 cells and adoptively transferred into *Rag2*$^{-/-}$ mice, followed by the inoculation of LM-phenotype cells.

(G) Schematics of the adoptive cell transfer model in immunocompetent mice.

(H) Representative immunofluorescence staining for leptomeningeal metastatic lesions in mice with indicated treatment (luciferase, green; DAPI, blue). The white line and arrows indicate the border of the metastatic lesions ($n$ = 6 per group). Scale bar = 50μm.

(I) Kaplan-Meier plots of overall survival of mice with indicated treatment. Black, PBS ($n$ = 12); blue, adoptive transfer of CD4$^+$ T cells ($n$ = 12, $P$ = 0.56 compared with mice treated with PBS); red, adoptive transfer of CD8$^+$ T cells ($n$ = 12, $P < 0.001$ compared with mice treated with PBS).

Figure 3.

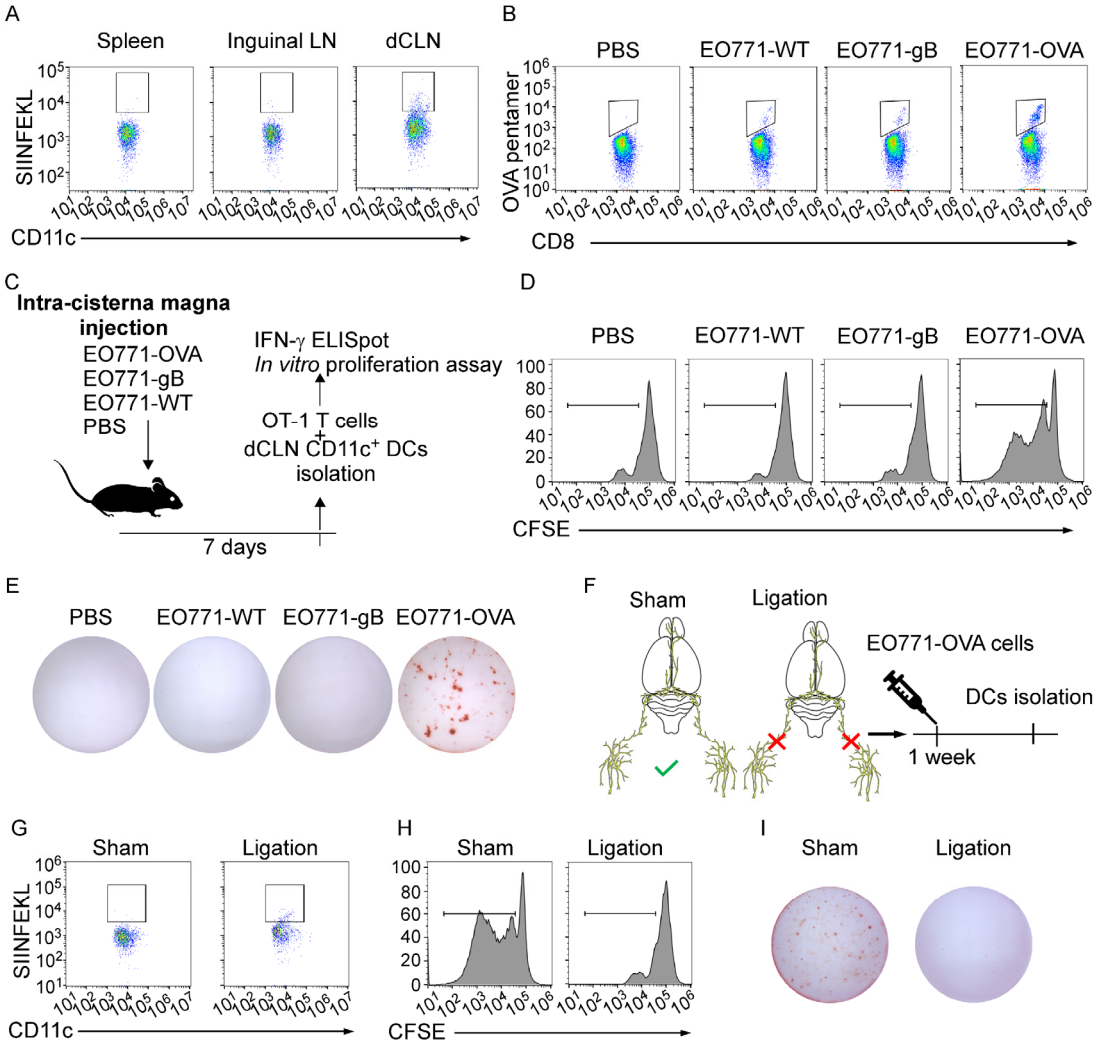


**Figure 3. dCLNs generate tumor-specific CD8$^+$ T cells against leptomeningeal metastasis.**

(A) DCs from spleen, inguinal LNs and dCLNs were isolated 7 days after intra cisterna magna EO771-OVA cell injection, and later analyzed for SIINFEKL presentation ($n$ = 8 per group).

(B) PBS, EO771 and EO771 expressed with gB (EO771-gB) and OVA (EO771-OVA) were injected into C57BL/6 mice. CD8$^+$ T cells from lymph nodes were isolated and later analyzed for OVA pentamer expression. ($n$ = 5 per group)

(C) Schematics of animal experiments detecting the generation of tumor-specific CD8$^+$ T cells *in vitro*. PBS, EO771 and EO771-gB and EO771-OVA were injected into C57BL/6 mice. DCs were subsequently isolated from dCLNs, and then co-cultured

with OT-1 T cells *in vitro*.

(D) Representative histogram of CFSE dilution of OT-1 T cells co-cultured with $CD11c^+$ cells isolated from dCLNs of mice with indicated treatment for 60 h. ($n$ =5 per group.)

(E) Representative images of IFN-γ ELISpot data of OT-1 T cells co-cultured with $CD11c^+$ cells isolated from dCLNs of mice with indicated treatment for 60 h ($n$ = 5 per group).

(F) Schematics of animal experiments illustrating dCLNs generate tumor-specific $CD8^+$ T cells against leptomeningeal metastasis. Surgical ligation of the lymphatics afferent to the dCLNs was performed. A week after the surgery, sham or ligation group were inoculated with EO771-OVA cells. DCs were subsequently isolated from dCLNs, and then co-cultured with OT-1 T cells *in vitro*.

(G) Representative histogram of SIINFEKL expression on $CD11c^+$ cells isolated from dCLNs of mice with indicated treatment ($n$ = 8 per group).

(H) Representative histogram of CFSE dilution of OT-1 T cells co-cultured with $CD11c^+$ cells isolated from dCLNs of mice with indicated treatment for 60 h ($n$ = 5 per group).

(I) Representative images of IFN-γ ELISpot data of OT-1 T cells co-cultured with $CD11c^+$ cells isolated from dCLNs of mice with indicated treatment for 60 h ($n$ = 4 per group).

Figure 4.

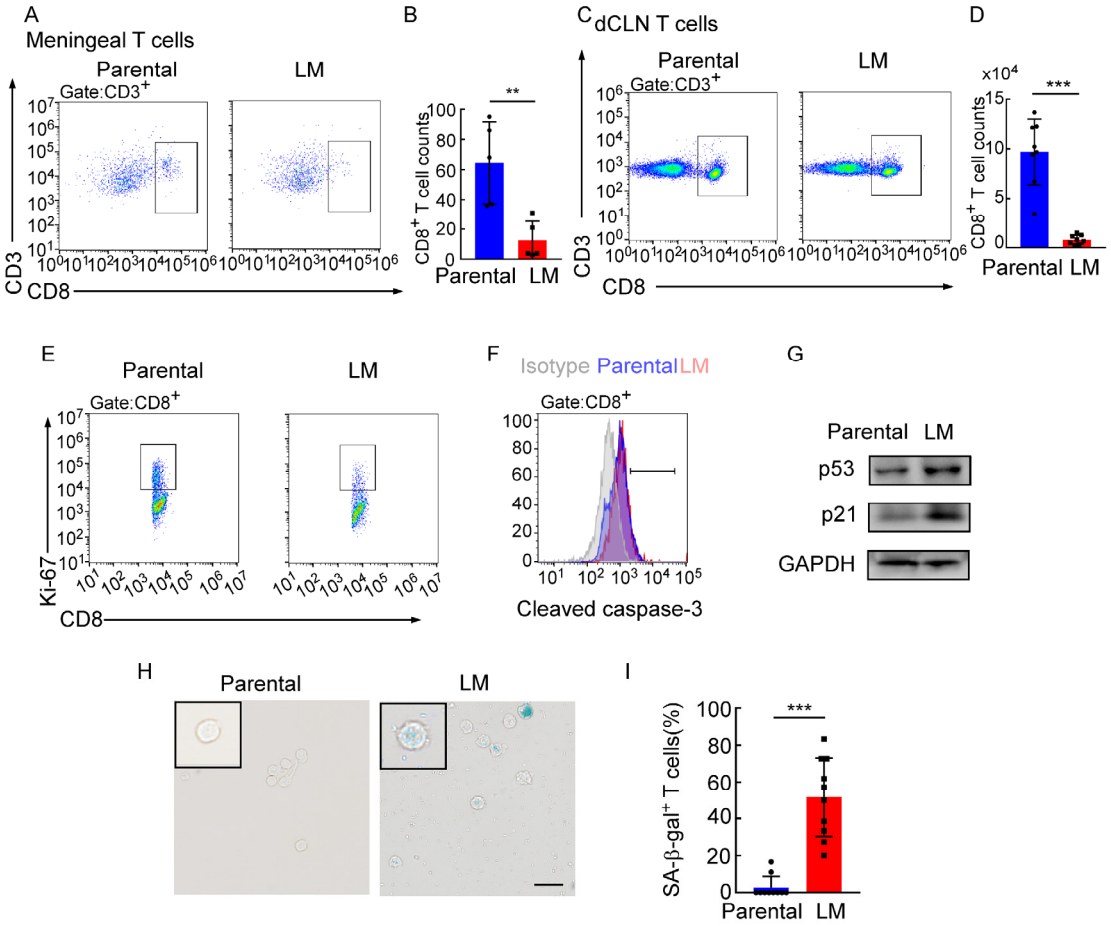


**Figure 4. dCLN CD8$^+$ T cells exhibit senescence in leptomeningeal metastasis.**

(A-I) $1 \times 10^5$ EO771 parental or LM-phenotype cells were inoculated into the intracarotid artery of recipient mice.

(A-B) T cells in the meninges were isolated from mice injected with EO771 parental and LM-phenotype cells and analyzed by flow cytometry. Representative images (A) and quantitation (B) of meningeal CD8$^+$ T cells in gated CD3$^+$ T cells were shown (mean ± SD, $n = 5$ per group). ** $P < 0.01$ by two-tailed Student's $t$ test.

(C-D) T cells in the dCLNs were isolated from mice injected with EO771 parental and LM-phenotype cells and analyzed by flow cytometry. Representative images (C) and quantitation (D) of dCLN CD8$^+$ T cells in gated CD3$^+$ T cells were shown (mean ± SD, $n = 5$ per group). *** $P < 0.001$ by two-tailed Student's $t$ test.

(E) Representative images of proliferative capacity of CD8$^+$ T cells isolated from

dCLNs, as determined by flow cytometry for the percentages of Ki-67$^+$ cells ($n$ = 4 per group).

(F) Representative histogram of apoptosis of CD8$^+$ T cells isolated from dCLNs, as determined by flow cytometry for the percentages of cleaved caspase-3$^+$ cells. Grey, isotype; blue, parental; red, LM ($n$ = 4 per group).

(G) Representative immunoblots for p53 and p21 in CD8$^+$ T cells isolated from dCLNs ($n$ = 4 per group).

(H-I) Representative images (H) and quantitation (I) of SA-β-gal staining in CD8$^+$ T cells isolated from dCLNs. Scale bar = 20μm (mean ± SD, $n$ = 10 per group). *** $P <$ 0.001 by two-tailed Student's $t$ test.

**Figure 4—source data 1. Uncropped blots of Figure 4G.**


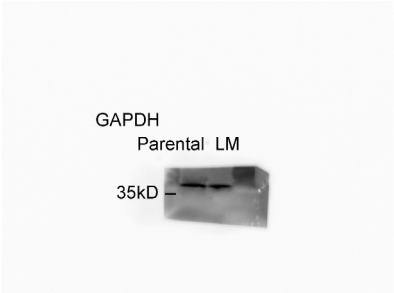

Figure 5.

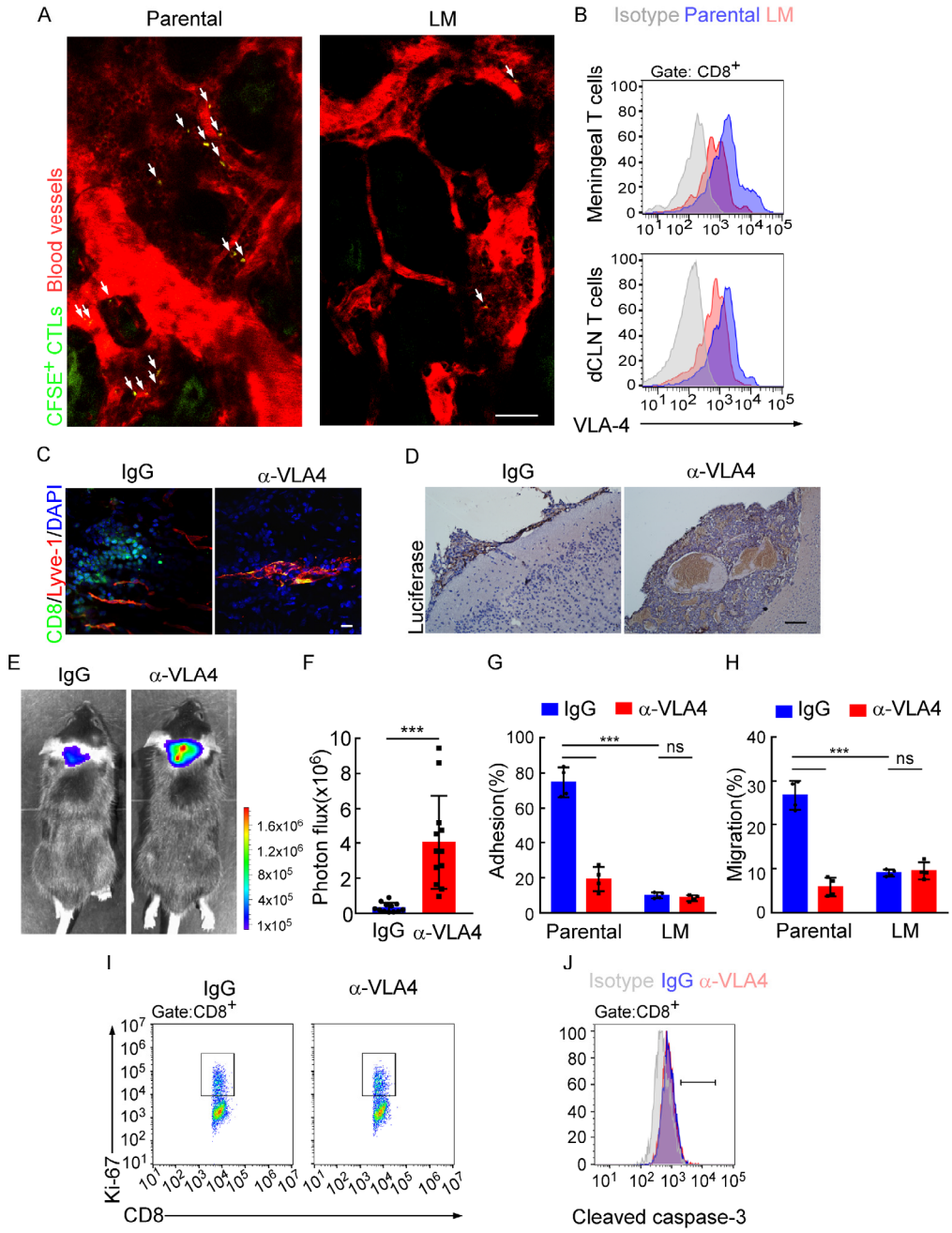


**Figure 5. Downregulation of VLA-4 in senescent CD8$^+$ T cells impairs their trafficking to meninges.**

(A) CD8$^+$ T cells were isolated from the dCLNs of mice injected with parental and LM-phenotype cells respectively, stained with CFSE, and subsequently transferred to the recipient mice. 24h after T cell transfusion, two photon imaging was used to reveal the *in vivo* migration of CFSE-labeled CTLs to meninges ($n$ = 4 per group). Visualization

of the vasculature by i.v. injection of Rhodamine-dextran (red). The location of $CFSE^+$ T cells (green) were marked by a white arrowhead. Scale bar, 50 μm.

(B) T cells in the meninges and dCLNs were isolated from mice injected with parental and LM-phenotype cells. Flow cytometry analysis of VLA-4 expression in $CD8^+$ T cells isolated from meninges (top) or dCLNs (bottom) of mice receiving parental or LM-phenotype cells. Grey, isotype; blue, Parental- $CD8^+$ T cells; red, LM-$CD8^+$ T cells.

(C-F) C57BL/6 mice pretreated with IgG or α-VLA-4 antibodies were injected with parental EO771-luc cells via intracarotid artery.

(C) Representative immunofluorescent images of meningeal $CD8^+$ T cells from C57BL/6 mice with indicated treatment in whole mount meninges. Scale bar = 50μm. Red, Lyve-1; green, CD8; blue, DAPI ($n$ = 5 per group).

(D) Representative IHC images for luciferase to identify leptomeningeal metastatic lesions. Scale bar = 50μm ($n$ = 5 per group).

(E-F) Representative bioluminescence images (E) and quantitation (F) of metastases in mice with indicated treatment at day 21 post-injection (mean ± SD, $n$ = 12 per group). *** $P < 0.001$ by two-tailed Student's $t$ test.

(G) $CD8^+$ T cells in dCLNs of mice injected with EO771 LM-phenotype cells or parental cells were isolated and tested for their ability to adhere to plate-bound VCAM-1-Ig fusion protein. Histogram shows the number of cells adherent to the bottom of the wells under indicated treatments(mean ± SD, $n$ = 4 per group). *** $P$ <0.001, ns, not significant by two-way ANOVA with Sidak's multiple comparison test.

(H) $CD8^+$ T cells isolated from mice injected with EO771 LM-phenotype cells or parental cells, were treated with IgG or VLA4 antibody and later added to the top chamber of *in vitro* blood-brain barrier model. Histogram indicates the number of migrated $CD8^+$ T cells after IgG or VLA4 antibody treatment(mean ± SD, $n$ = 4 per group). *** $P$ <0.001, ns not significant by two-way ANOVA with Sidak's multiple comparison test.

(I) Representative images of proliferative capacity of dCLN $CD8^+$ T cells under indicated treatment, as determined by flow cytometry for the percentages of Ki-$67^+$

cells ($n$ = 4 per group).

(J) Representative histogram of apoptosis of dCLN $CD8^+$ T cells under indicated treatment, as determined by flow cytometry for the percentages of cleaved caspase-$3^+$ cells. Grey, isotype; blue, IgG antibody; red, VLA-4 antibody ($n$ = 4 per group).

1068

Figure 6.

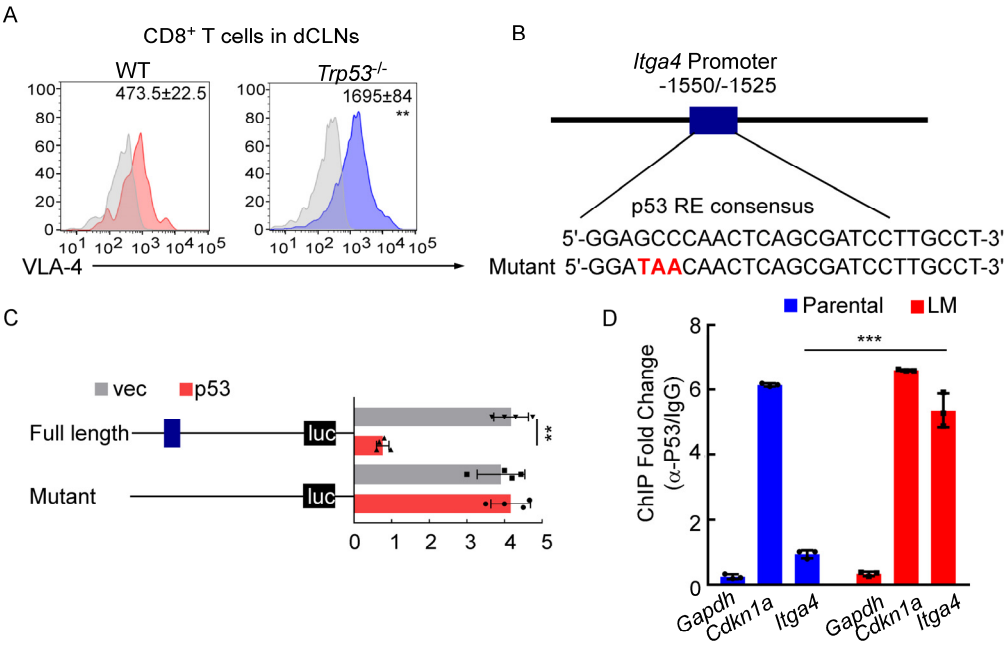


1069

1070 **Figure 6. VLA-4 transcription is repressed by p53.**

1071 (A) $CD8^+$ T cells were isolated from dCLNs of WT or *Trp53*$^{-/-}$ mice injected with LM-

1072 phenotype cells. Flow cytometry analysis of VLA-4 expression in $CD8^+$ T cells from

1073 dCLNs in WT mice or *Trp53*$^{-/-}$ mice receiving LM-phenotype cells. Grey, isotype; blue,

1074 $CD8^+$ T cells from WT mice; red, $CD8^+$ T cells from *Trp53*$^{-/-}$mice. Numbers in plot

1075 correspond to the mean fluorescent intensity of VLA-4 in $CD8^+$ T cells (mean ± SD,

1076 $n = 4$ per group). $^{**}P < 0.01$ compared with $CD8^+$ T cells from WT mice by two-tailed

1077 Student's *t* test.

1078 (B) A schematic of *Itga4* gene promoter. P53 binding site is identified.

1079 (C) EL4 cells were transfected with wild type or a mutant version in which the putative

1080 p53 binding site was mutated with four nucleotides (mutant). Afterwards, EL4 cells

1081 were transfected with empty vector or P53 overexpression plasmids and harvested for

1082 the luciferase activity assay (mean ± SD, $n = 4$). Results are expressed relatively to

1083 control conditions. ** $P \leq 0.01$ by one-way ANOVA with Tukey's multiple comparison

1084 test.

(D) ChIP was performed with a p53-targeting antibody or a control IgG to assess p53 binding to the *Itga4* promoter in $CD8^+$ T cells isolated from mice injected with parental or LM-phenotype cells (mean ± SD, $n = 3$). *Cdkn1a* serves as a positive control, *Gapdh* as a negative control for p53 binding. *** $P < 0.001$ by two-tailed Student's *t* test.

Figure 7.

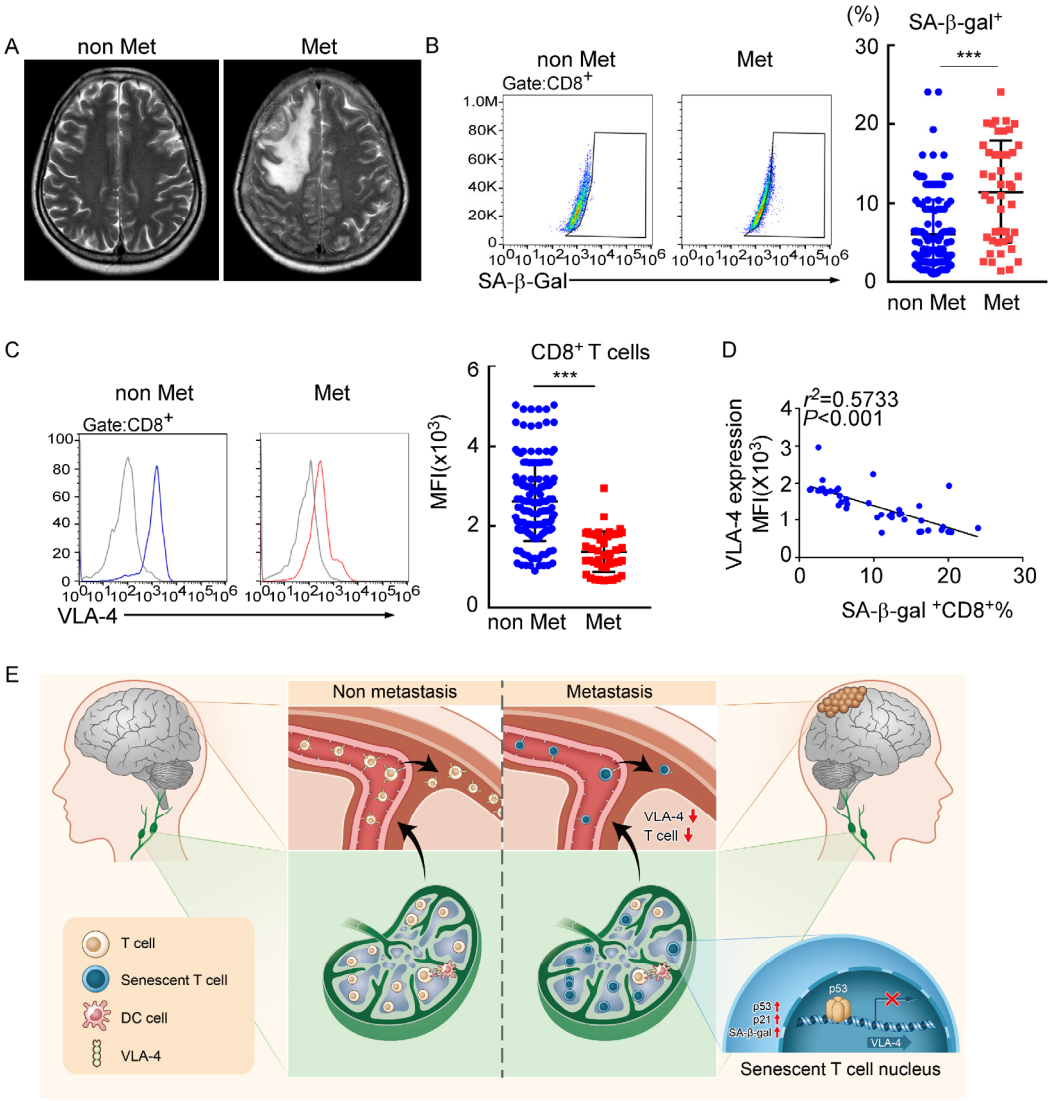


**Figure 7. Meningeal CD8$^+$ T cells exhibit VLA-4 downregulation and senescence in human leptomeningeal metastasis.**

(A) Representative MRI images of patients with ($n$ = 45) or without leptomeningeal metastases ($n$ = 145).

(B) Representative images for flow cytometry analysis of CD8$^+$SA-β-gal$^+$ T cells from CSF in patients of non-malignant neurological diseases ($n$ = 145) or leptomeningeal metastasis ($n$ = 45). Bars correspond to the percentages of CD8$^+$SA-β-gal$^+$ T cells. *** $P < 0.001$ by two-tailed Student's $t$ test.

(C) Flow cytometry analysis of VLA-4 expression in CD8$^+$ T cells from CSF in patients of non-malignant neurological diseases ($n$ = 145) or leptomeningeal metastasis ($n$ = 45).

Grey, isotype; blue, $CD8^+$ T cells in patients of non-malignant neurological diseases; red, $CD8^+$ T cells in leptomeningeal metastasis patients. Bars correspond to the mean fluorescent intensity (MFI) of VLA-4 in $CD8^+$ T cells. *** $P < 0.001$ by two-tailed Student's *t* test.

(D) The correlation between the percentages of SA-β-$gal^+CD8^+$ T cells and VLA-4 levels in $CD8^+$ T cells of leptomeningeal metastatic patients ($n = 45$, the Pearson's correlation coefficient $r^2$ value and the *P* value are shown).

(E) Schematics highlighting the major findings of this study.

Figure supplement 1.

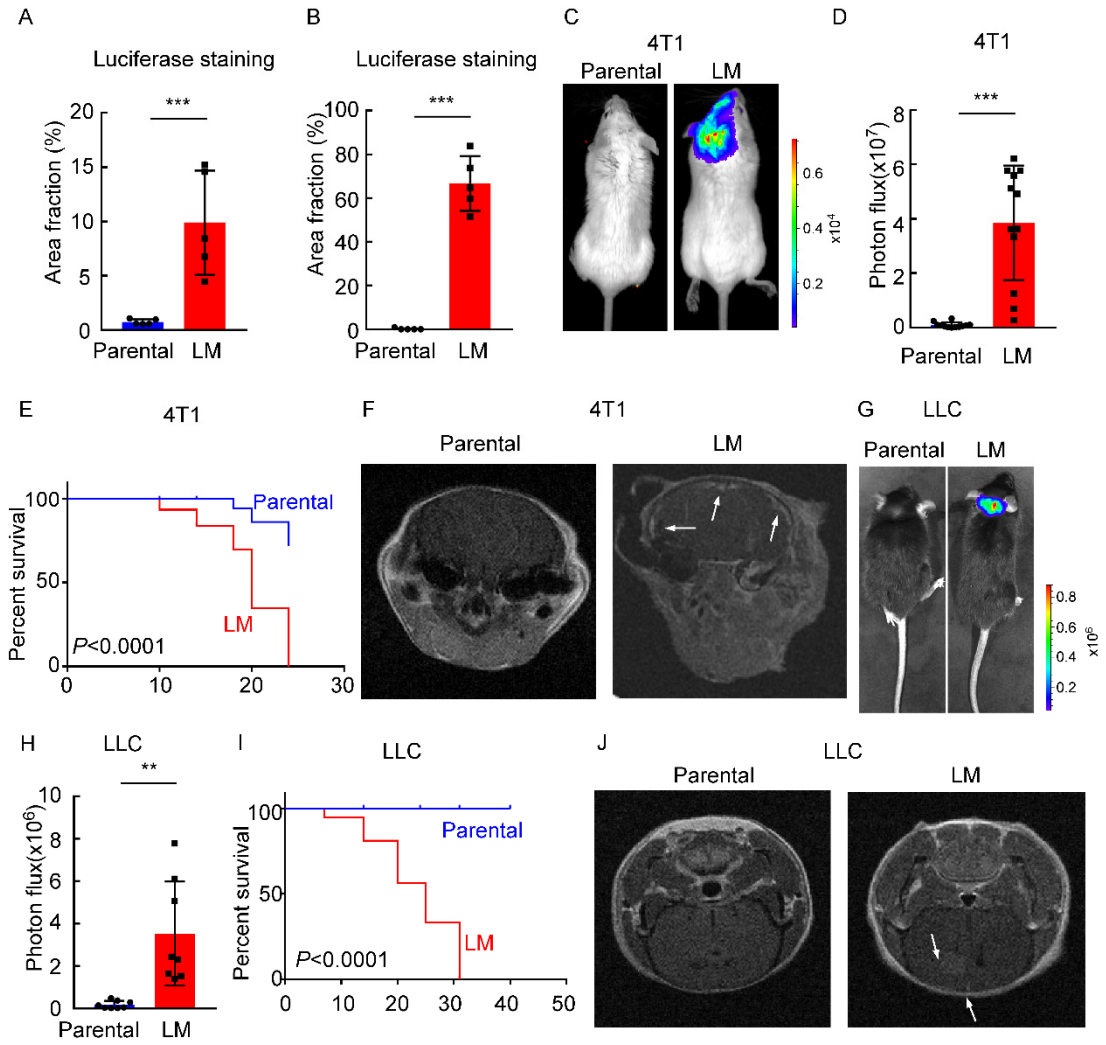


**Figure supplement 1. Establishing a model of leptomeningeal metastasis.**

(A) Quantification of Figure 1E (mean ± SD, $n = 5$ per group). *** $P < 0.001$ by two-tailed Student's $t$ test.

(B) Quantification of Figure 1F (mean ± SD, $n = 5$ per group). *** $P < 0.001$ by two-tailed Student's $t$ test.

(C-F) $1\times10^5$ 4T1 parental or LM-phenotype cells were inoculated into the intracarotid artery of recipient mice.

(C) Representative BLI images were shown.

(D) Histogram represents *in vivo* BLI imaging at day 28 post-injection (mean ± SD, $n = 12$ per group.). *** $P < 0.001$ by two-tailed Student's $t$ test.

(E) Kaplan-Meier plot of overall survival of mice.

(F) MRI at day 28 post-inoculation revealed leptomeningeal metastasis was formed after LM-phenotype cell inoculation. The white arrows indicate metastatic lesions.

(G-J) $1\times10^5$ LLC parental or LM-phenotype cells were inoculated into the intracarotid artery of recipient mice.

(G) Representative BLI images were shown.

(H) Histogram represents *in vivo* BLI imaging at day 28 post-injection (mean ± SD, $n$ = 8 per group.). ** $P < 0.01$ by two-tailed Student's $t$ test.

(I) Kaplan-Meier plot of overall survival of mice.

(J) MRI at day 28 post-inoculation revealed leptomeningeal metastasis was formed after LM-phenotype cell inoculation. The white arrows indicate metastatic lesions.

Figure supplement 2.

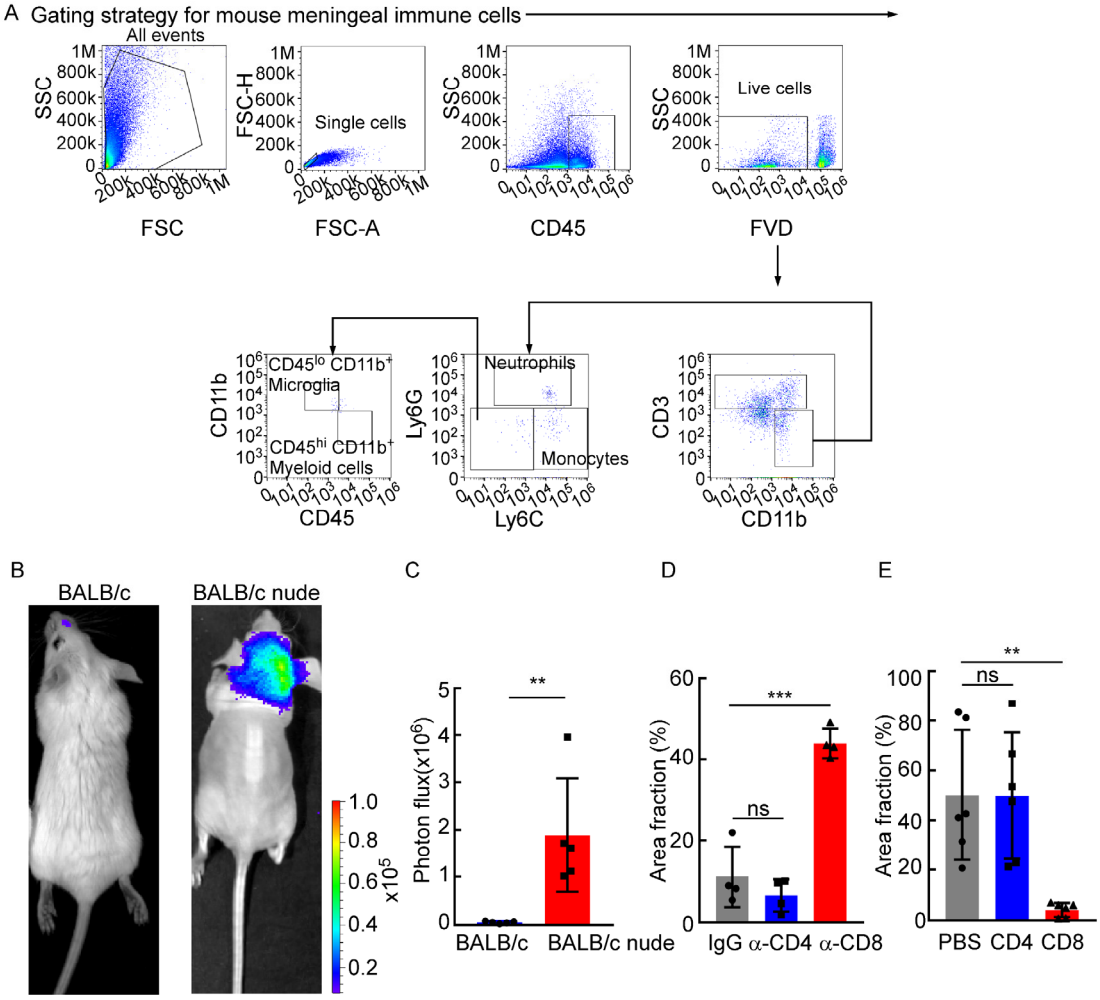


**Figure supplement 2. CD8$^+$ T cells play a role in constraining intracranial tumor growth.**

(A) The gating strategy for mouse meningeal immune cells in Figure 2A-B.

(B-C) $1\times10^5$ 4T1 LM-phenotype cells were injected into the intracarotid artery of wild type BABL/c or BALB/c nude mice.

(B) Representative bioluminescence images for tumor growth of wild type BALB/c and BALB/c nude mice monitored by BLI ($n$ = 5 per group).

(C) Histogram represents *in vivo* BLI imaging at day 28 post-injection (mean ± SD, $n$ = 5 per group). ** $P < 0.01$ by two-tailed Student's $t$ test.

(D) Comparison of tumor area in Figure 2E (H&E, mean ± SD, $n$ = 4 per group). ns not significant, *** $P < 0.001$ by one-way ANOVA with Tukey's multiple comparison test.

(E) Comparison of tumor area in Figure 2H (IF, mean ± SD, $n$ = 6 per group). ns not

significant, ** $P < 0.01$ by one-way ANOVA with Tukey's multiple comparison test.

Figure supplement 3.

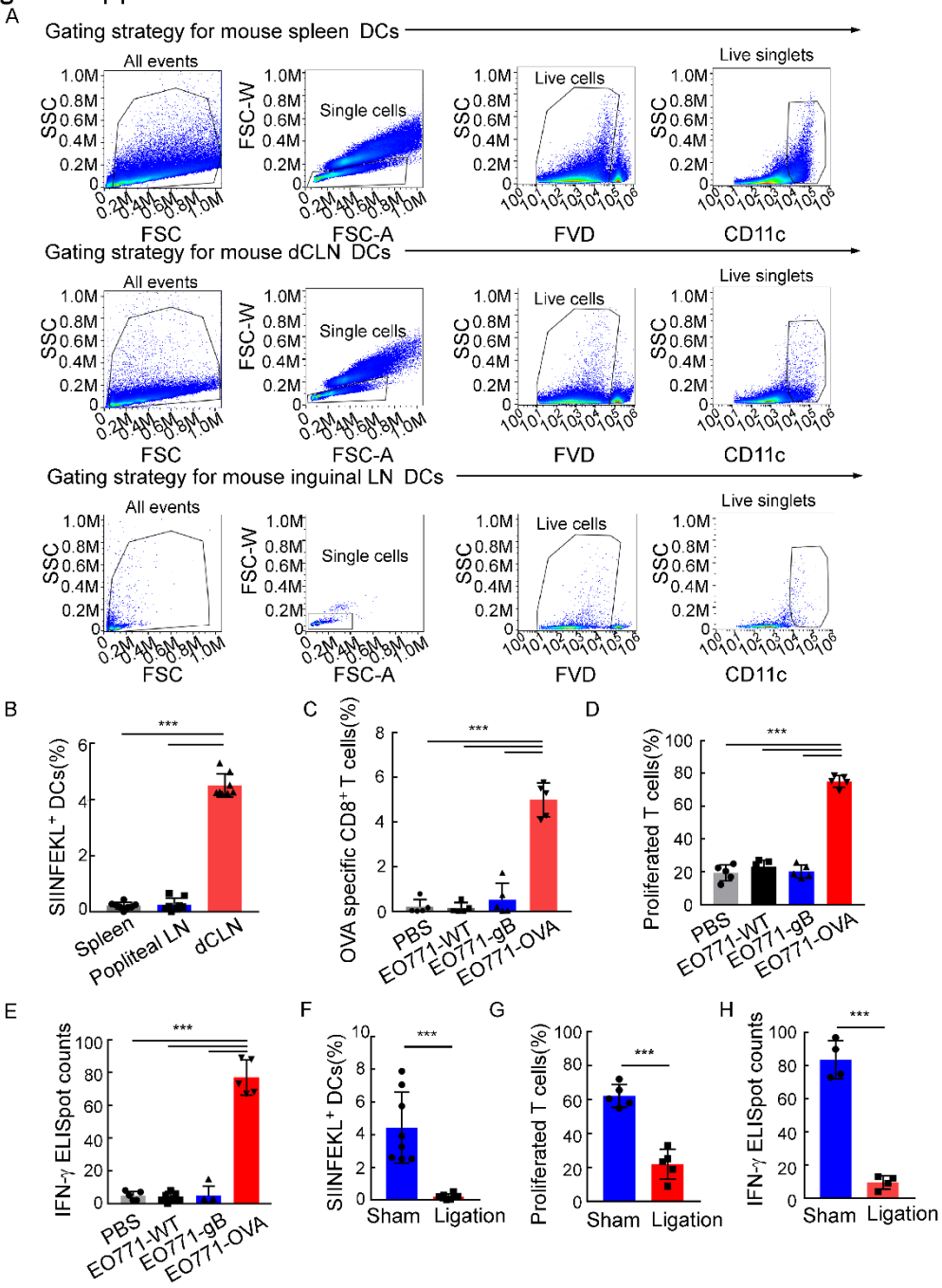


**Figure supplement 3. dCLNs generate antigen-specific CD8$^+$ T cells against leptomeningeal metastasis.**

(A) The gating strategy for mouse DCs in Figure 3A.

(B) Quantification of Figure 3A (mean ± SD, $n$ = 8 per group). *** $P < 0.001$ by one-way ANOVA with Tukey's multiple comparison test.

(C) Quantification of Figure 3B (mean ± SD, $n$ = 5 per group). *** $P < 0.001$ by one-way ANOVA with Tukey's multiple comparison test.

(D) Quantification of Figure 3D (mean ± SD, $n = 5$ per group). *** $P < 0.001$ by one-way ANOVA with Tukey's multiple comparison test.

(E) Quantification of Figure 3E (mean ± SD, $n = 5$ per group). *** $P < 0.001$ by one-way ANOVA with Tukey's multiple comparison test.

(F) Quantification of Figure 3G (mean ± SD, $n = 8$ per group). *** $P < 0.001$ by two-tailed Student's *t* test.

(G) Quantification of Figure 3H (mean ± SD, $n = 5$ per group). *** $P < 0.001$ by two-tailed Student's *t* test.

(H) Quantification of Figure 3I (mean ± SD, $n = 4$ per group). *** $P < 0.001$ by two-tailed Student's *t* test.

Figure supplement 4.

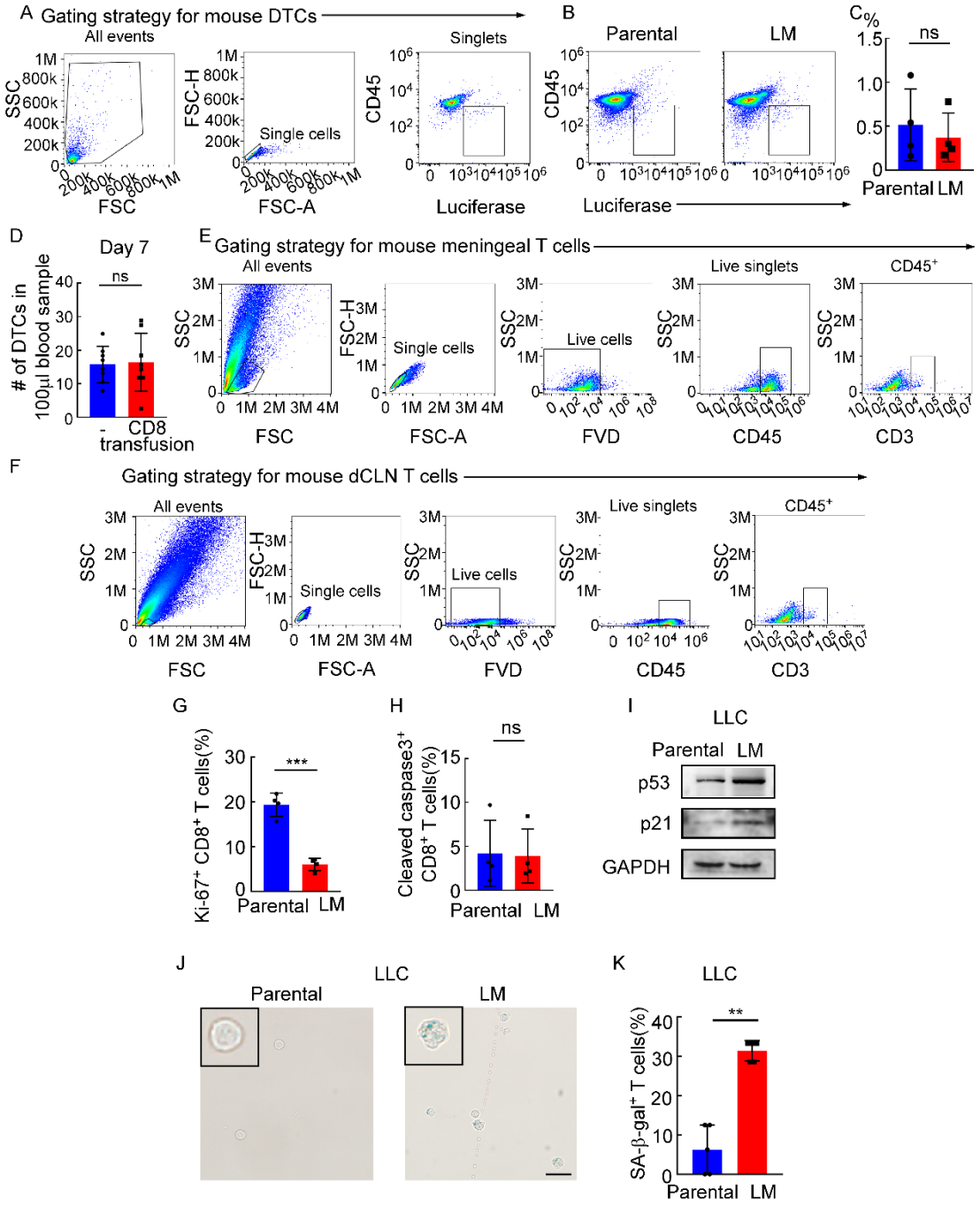


**Figure supplement 4. Meningeal CD8$^+$ T cells which show cell cycle arrest undergo senescence instead of apoptosis under leptomeningeal metastasis.**

(A) The gating strategy for mouse DTCs in Figure supplement 4B.

(B) DTCs from mice injected with EO771 parental or LM cells analyzed by flow cytometry (DTCs defined as CD45$^-$luciferase$^+$).

(C) Quantification of Figure supplement 4B (mean ± SD, *n* = 4 per group). ns not

significant by two-tailed Student's *t* test.

(D) Histogram indicates the number of DTCs of 100 μl peripheral blood in *Rag2*$^{-/-}$ mice without or with CD8$^+$ T cell transfusion. ns not significant (mean ± SD, $n = 8$ per group) by two-tailed Student's *t* test.

(E) The gating strategy for mouse CD3$^+$ T cells in Figure 4A.

(F) The gating strategy for mouse CD3$^+$ T cells in Figure 4C.

(G) Quantification of Figure 4E (mean ± SD, $n = 4$ per group). *** $P < 0.001$ compared with dCLN Parental-CD8$^+$ T cells by two-tailed Student's *t* test.

(H) Quantification of Figure 4F (mean ± SD, $n = 4$ per group). ns not significant compared with dCLN Parental-CD8$^+$ T cells by two-tailed Student's *t* test.

(I-K) $1\times10^5$ LLC parental or LM-phenotype cells were inoculated into the intracarotid artery of recipient mice.

(I) Representative immunoblots for p53 and p21 in CD8$^+$ T cells isolated from dCLNs ($n = 3$ per group).

(J) Representative images of SA-β-gal staining in CD8$^+$ T cells isolated from dCLNs. Scale bar = 20μm ($n = 5$ per group).

(K) Histogram indicates the proportion of senescent CD8$^+$ T cells isolated from mice with indicated treatment(mean ± SD, $n = 5$ per group). ** $P < 0.01$ compared with dCLN Parental-CD8$^+$ T cells by two-tailed Student's *t* test.

**Figure supplement 4—source data 2. Uncropped blots of Figure supplement 4I.**

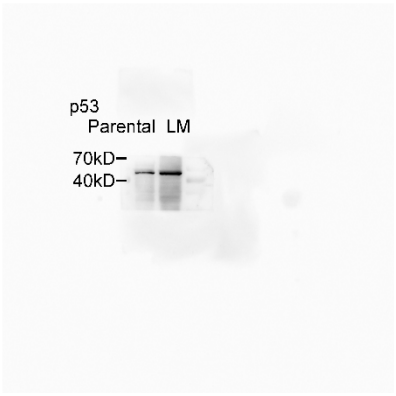


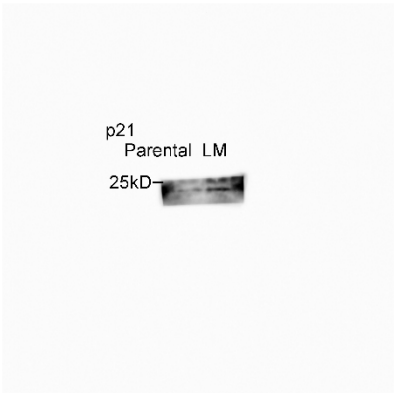


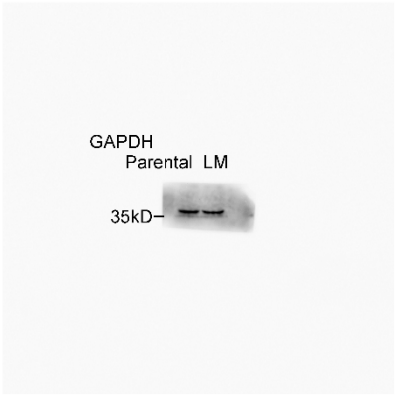

Figure supplement 5.

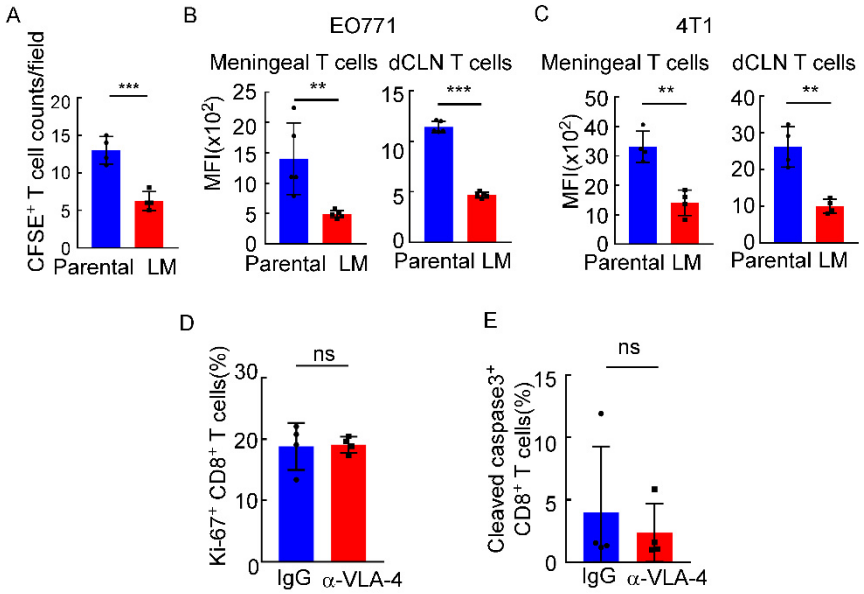


**Figure supplement 5. Downregulated VLA-4 in CTLs inhibits their recruitment to meninges and their capacity to control leptomeningeal metastasis.**

(A) Quantification of Figure 5A (mean ± SD, $n = 4$ per group). *** $P < 0.001$ compared with meningeal Parental-CD8$^+$ T cells by two-tailed Student's $t$ test.

(B) Quantification of Figure 5B (mean ± SD, $n = 5$ per group). ** $P < 0.01$, *** $P < 0.001$ compared with meningeal/ dCLN Parental-CD8$^+$ T cells by two-tailed Student's $t$ test.

(C) T cells in the meninges and dCLNs were isolated from mice injected with 4T1 parental and LM-phenotype cells. Flow cytometry analysis of VLA-4 expression in CD8$^+$ T cells isolated from meninges and dCLNs of mice receiving parental or LM-phenotype cells. Histogram indicates the mean fluorescence intensity of anti-VLA-4 staining (mean± SD, $n = 4$ per group). ** $P < 0.01$ compared with meningeal/ dCLN Parental-CD8$^+$ T cells by two-tailed Student's $t$ test.

(D) Quantification of Figure 5I (mean ± SD, $n = 4$ per group). ns not significant compared with dCLN T cells from mice injected with IgG by two-tailed Student's $t$ test.

(E) Quantification of Figure 5J (mean ± SD, $n = 4$ per group). ns not significant compared with dCLN T cells from mice injected with IgG by two-tailed Student's $t$ test.

Figure supplement 6.

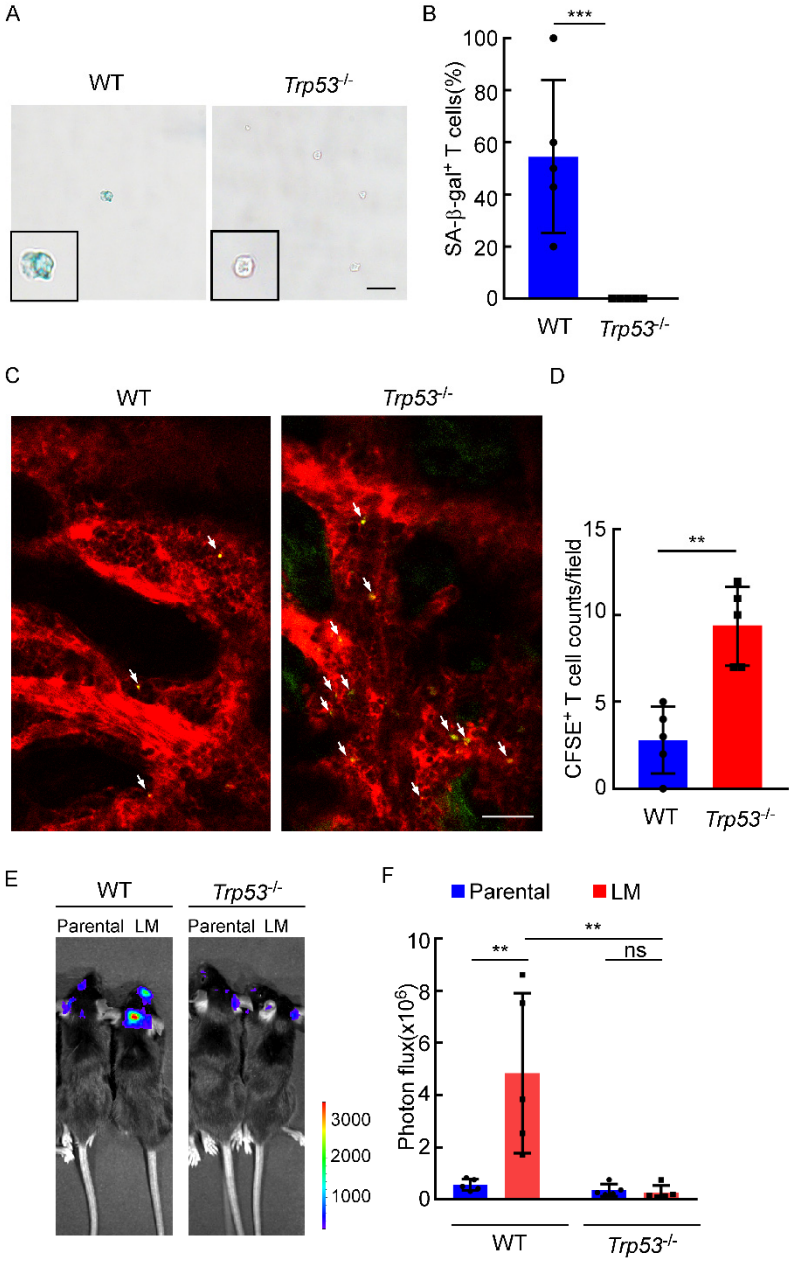


**Figure supplement 6. The role of P53 in leptomeningeal metastasis.**

(A-B) Representative images (A) and quantitation (B) of SA-β-gal staining in $CD8^+$ T cells isolated from dCLNs of WT or *Trp53*$^{-/-}$ mice injected with LM cells. Scale bar = 20μm (mean ± SD, $n$ = 5 per group.). *** $P < 0.001$ compared with dCLN T cells isolated from WT mice by two-tailed Student's $t$ test.

(C-D) Representative two-photon imaging(C) and quantitation(D) of meninges of C57BL/6 or *Trp53*$^{-/-}$ mice receiving CFSE-labeled T cell transfusion (mean ± SD, $n$ =

5 per group). ** $P < 0.01$ by two-tailed Student's *t* test.

(E-F) Representative images (E) and quantitation (F) for tumor growth of WT C57BL/6 and *Trp53*$^{-/-}$ mice injected with EO771 parental or LM cells monitored by BLI (mean ± SD, $n = 5$ per group). ns, not significant; ** $P < 0.01$ by two-way ANOVA with Tukey's multiple comparison test.

Figure supplement 7.

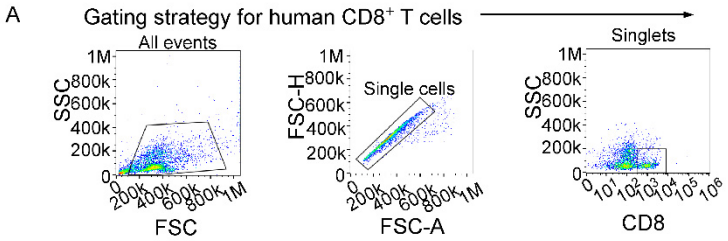


**Figure supplement 7. The relationship between VLA-4 downregulation and senescence in meningeal CD8$^+$ T cells in human leptomeningeal metastasis.**

(A) The gating strategy for human CD8$^+$ T cells from CSF in Figure 7B-C.